
C
S
P

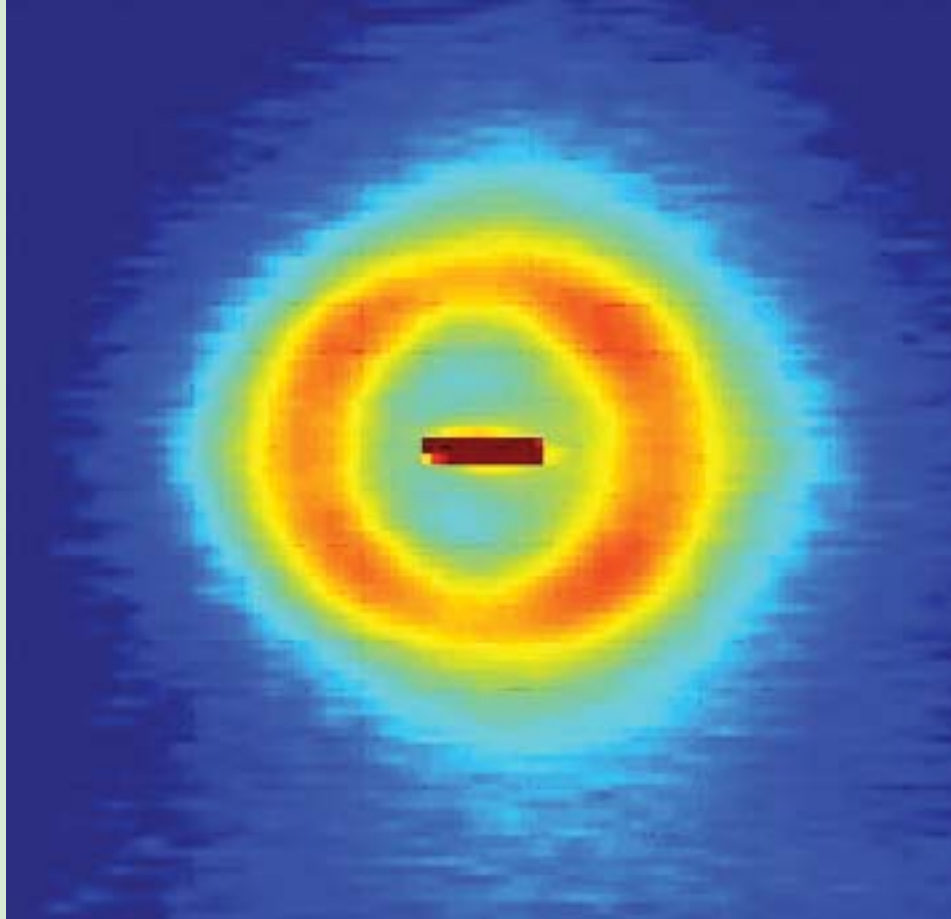
The DOE Center of Excellence for the
Synthesis and Processing
of Advanced Materials



BASIC ENERGY SCIENCES
DIVISION OF MATERIALS SCIENCES
& ENGINEERING

Member Laboratories: Ames Laboratory, Argonne National Laboratory, Brookhaven National Laboratory, Idaho National Engineering and Environmental Laboratory, University of Illinois Frederick Seitz Materials Research Laboratory, Lawrence Berkeley National Laboratory, Lawrence Livermore National Laboratory, Los Alamos National Laboratory, National Renewable Energy Laboratory, Oak Ridge National Laboratory, Pacific Northwest National Laboratory, and Sandia National Laboratories

Research Briefs



For questions and additional information contact:

George A. Samara
Sandia National Laboratories/NM
Phone: (505) 844-6653
Fax: (505) 844-4045
E-mail: gasamar@sandia.gov

C
S
P

The DOE Center of Excellence for the
Synthesis and Processing
of Advanced Materials



BASIC ENERGY SCIENCES
DIVISION OF MATERIALS SCIENCES
& ENGINEERING

Research Briefs

October 2003

Table of Contents

Preface	4
The Center's Member Laboratories	6
Membership of the Technology Steering Group	6
Center Projects and Their Coordinators	7
Executive Summary	8

Research Briefs

Isolated and Collective Phenomena in Nanocomposite Magnets	18
• Interfacial Modification in Nanocomposite Permanent Magnets	18
• Epitaxy and Residual Stress Induced Changes on the Curie Temperature of Nd ₂ Fe ₁₄ B	20
• Ferro-/Antiferro-Magnetic Competition in FePt Alloys	22
Smart Structures Based on Electroactive Polymers	24
• Approaches to Self-Assembled Nanoscale Materials with High Porosity	24
• Induced Ordering Phenomena in Block Co-Polymer Systems	26
• Hydrogel-Water Interactions for Sensing and Controlled Release	28
• Characterization of Electrochemically-Active Block Copolymers	30
Nanoscale Phenomena in Perovskite Thin Films	32
• Limit of Ferroelectricity in Ultra-Thin Perovskite PbTiO ₃ Films Identified by <i>In Situ</i> Synchrotron X-ray Scattering Studies	32
• Studies of Ferroelectric Phenomena in Perovskite Nanostructures	34
• High Energy Density/High Zirconia Content PLZT Films	36
The Science of Localized Corrosion	38
• Nano-void Nucleation and Growth at the Aluminum/Oxide Interface as a Pre-pitting Process	38

Table of Contents

• The Kinetics of Al ₂ O ₃ Film Dissolution in Aqueous Chloride Solutions	40
• <i>Ab Initio</i> Modeling of Electrochemical Interfaces: The Double Layer and H ₂ O Reduction on Cu(111)	42
• <i>Ab Initio</i> Modeling of Electrochemical Interfaces: Underpotential Oxidation of Cu(111) in H ₂ O	44
Controlled Defect Structures in Rare-Earth-Ba-Cu-O Cuprate Superconductors	46
• Intrinsic and Materials Effects on the Thickness Dependence of J _c in YBCO Coated Conductors	46
• AC Losses in Circular Disks of YBa ₂ Cu ₃ O ₇ Films in Perpendicular Magnetic Fields	48
• Reel-to-Reel Characterization of Time-Based Phase Evolution in YBCO Coated Conductors: The BaF ₂ Precursor	50
Carbon-Based Nanostructured Materials	52
• Low-Temperature Growth of Ultrananocrystalline Diamond Thin Films	52
• Nanotribology and Surface Chemistry of Carbon-Based Films	54
• The Effect of Load on Friction and Wear in Hard Carbon Thin Films for MEMS	56
Granular Flow and Kinetics	58
• Electrostatically Driven Granular Media	58
• Forces in Granular Hopper Flow	60
• Granular Chains: Dynamics of Nonequilibrium Polymers	62
Experimental and Computational Lubrication at the Nanoscale	64
• Friction between Disordered Self-Assembled Alkylsilane Monolayers	64
• Experimentally-Determined Structure and Dynamics in Confined Fluids	66
• Control of Friction at the Nanoscale	68

Preface

This publication, *Research Briefs*, is designed to inform present and potential customers and partners of the DOE Center of Excellence for the Synthesis and Processing of Advanced Materials (CSP) about significant advances resulting from Center-coordinated research. The format for *Research Briefs* is an easy-to-read, not highly technical, concise presentation of the accomplishments. Each *Brief* provides a statement of the motivation for the research followed by a description of the accomplishment and its significance.

The Center is a distributed center for promoting coordinated, collaborative research partnerships related to the synthesis and processing of advanced materials. It was established by the Department of Energy's Division of Materials Sciences and Engineering, Office of Basic Energy Sciences and the DOE Laboratories in recognition of the enabling role of materials synthesis and processing to numerous materials fabrication- and manufacturing-intensive technologies. The participants include investigators from 12 DOE national laboratories, universities and the private sector. The Center has a technology perspective provided by a Technology Steering Group.

By bringing together synergistic activities and capabilities in selected focus areas of materials synthesis and processing, the Center's goal is to be a vehicle for providing added value and making impact. The Center is also allowing better coordinated strategic planning by the Division of Materials Sciences and Engineering and the Laboratories and faster response time to special needs and opportunities. Additionally, the Center is serving as a model of R and D integration within the Department of Energy as well as a model of cooperation and collaboration among the participating institutions.

The overall objective of the Center is,

To enhance the science and engineering of materials synthesis and processing in order to meet the programmatic needs of the Department of Energy and to facilitate the technological exploitation of materials.

Synthesis and processing (S&P) are those essential elements of Materials Science and Engineering (MS&E) that deal with (1) the assembly of atoms or molecules to form materials, (2) the manipulation and control of the structure at all levels from the atomic to the macroscopic scale, and (3) the development of processes to produce materials for specific applications. Clearly, S&P represent a

large area of MS&E that spans the range from fundamental research to technology. The goal of basic research in this area ranges from the creation of new materials and the improvement of the properties of known materials, to the understanding of such phenomena as diffusion, interfacial phenomena, crystal growth, sintering, phase transitions, to the development of novel diagnostic, modeling and processing approaches, etc. On the applied side, the goal of S&P is to translate scientific results into useful materials by developing processes capable of producing high quality, cost-effective products.

The technical emphasis of the Center is on a number of focused multilaboratory projects which draw on the complementary strengths of the member institutions in their ongoing research programs. These projects were selected on the basis of the following criteria:

- scientific excellence
- clear relationship to energy technologies
- involvement of several laboratories
- existing or potential partnerships with DOE Technologies-funded programs
- existing or potential "in-kind" partnerships with industry

Each Project is coordinated by a knowledgeable representative from one of the participating laboratories. The Projects covered in this issue of *Research Briefs* and their Coordinators are listed in the accompanying table (p. 7). A few selected accomplishments from each of the Projects are presented. An Executive Summary provides highlights of these accomplishments organized by Project. Readers are encouraged to contact any of the Coordinators for information about the Center and its accomplishments.

One of the projects listed in the table on page 7, namely, *The Science of Localized Corrosion*, graduated at the end of FY2003. It has been replaced by the new Project, *Spin-Polarized Transport in Complex Oxides* which started at the beginning of FY2004. Center Projects are graduated after achieving their objectives, but no later than five years after start.

George A. Samara
October 2003

The Center's Member Laboratories

The member laboratories of the Center are:

- Ames Laboratory (Ames)
- Argonne National Laboratory (ANL)
- Brookhaven National Laboratory (BNL)
- Idaho National Engineering and Environmental Laboratory (INEEL)
- University of Illinois Frederick Seitz Materials Research Laboratory (UI/MRL)
- Lawrence Berkeley National Laboratory (LBNL)
- Lawrence Livermore National Laboratory (LLNL)
- Los Alamos National Laboratory (LANL)
- National Renewable Energy Laboratory (NREL)
- Oak Ridge National Laboratory (ORNL)
- Pacific Northwest National Laboratory (PNNL)
- Sandia National Laboratories (SNL)

Membership of the Technology Steering Group

<u>Member</u>	<u>Affiliation</u>
Prof. L. Eric Cross	Pennsylvania State University
Dr. David W. Johnson, Jr.	Agere Systems
Dr. Hylan B. Lyon	Marlow Industries
Dr. Christian Mailhot	DOE/Defense Programs; Lawrence Livermore National Laboratory
Dean Paul S. Peercy	University of Wisconsin
Dr. Udaya Rao	DOE/Fossil Energy
Dr. Charles Sorrell	DOE/Energy Efficiency & Renewable Energy
Dr. John Stringer	Electric Power Research Institute (EPRI)
Dr. Arthur Yang	Arthur Yang Industrial Science and Technology Network, Inc.

Center Projects Covered In This Issue Of *Research Briefs* and Their Coordinators

Project	Coordinator(s)
Isolated and Collective Phenomena in Nanocomposite Magnets	Samuel D. Bader (ANL) Phone: (630) 252-4960 E-mail: bader@anl.gov
Smart Structures Based on Electroactive Polymers	Gregory J. Exarhos (PNNL) Phone: (509) 375-2440 E-mail: greg.exarhos@pnl.gov
Nanoscale Phenomena in Perovskite Thin Films	Orlando Auciello (ANL) Phone: (630) 252-1685 E-mail: auciello@anl.gov and Duane Dimos (SNL/NM) Phone: (505) 844-6385 E-mail: dbdimos@sandia.gov
The Science of Localized Corrosion	Kevin Zavadil (SNL/NM) Phone: (505) 845-8442 E-mail: krzavad@sandia.gov
Controlled Defect Structures in Rare-Earth-Ba-Cu-O Cuprate Superconductors	David O. Welch (BNL) Phone: (631) 344-3517 E-mail: dwelch@bnl.gov
Carbon-Based Nanostructured Materials	John Carlisle (ANL) Phone: (630) 252-3520 E-mail: carlisle@anl.gov and Thomas Friedmann (SNL/NM) Phone: (505) 844-6684 E-mail: tafried@sandia.gov
Granular Flow and Kinetics	Shankar Subramaniam (Ames) Phone: (515) 294-3698 E-mail: shankar@iastate.edu
Experimental and Computational Lubrication at the Nanoscale	Steve Granick (UI/MRL) Phone: (217) 333-5720 E-mail: sgranick@uiuc.edu
Overall Center Coordinator	George A. Samara (SNL/NM) Phone: (505) 844-6653 E-mail: gasamar@sandia.gov

Executive Summary

The *Research Briefs* presented in this publication are intended to inform the Center's present and potential customers and partners about significant advances resulting from Center-coordinated research. Selected accomplishments from each of the eight Center focused projects are presented. This Executive Summary states the overall objective of each project followed by highlights of the accomplishments presented later in more detail.

Isolated and Collective Phenomena in Nanocomposite Magnets

Objective

Develop improved understanding of magnetic properties as well as improved magnetic materials using nanoscale mixtures of hard magnets, soft magnets and non-magnetic materials.

Highlights

- Interfacial modification by thermal annealing in two hard/soft, exchange-spring coupled nanocomposite permanent magnet systems, CoPt/Co and Sm-Co/Fe, has resulted in large changes in magnetic properties that point to a pathway for developing a new generation of nanocomposite magnets. (p. 18)
- The strong epitaxy observed between the (006) planes of Nd₂Fe₁₄B and the (110) planes of α -Fe in Nd₂Fe₁₄B/Fe magnetic nanocomposites results in large temperature-induced stresses in both materials. These stresses have a significant influence on magnetic properties (p. 20)
- First-principles spin model calculations have shown that the ground state for FePt nanoparticles and nanowires is antiferromagnetic and not ferromagnetic as found experimentally. Furthermore, the ferromagnetic state can be stabilized by anti-site defects (disorder) and enhanced tetragonality (c/a) of the crystal structure by alloying. (p. 22)

Smart Structures Based on Electroactive Polymers

Objective

Develop a framework for the rational design of self-assembled nanostructured block copolymers that offer significant advantages over conventional materials for the active regulation of transport phenomena.

Highlights

- A ball-and-stick model synthesis approach is used to impart strength and structure to a highly porous polymer network. A dendrimer core (organic aerogel) is combined with a rigid rod spacer to form a hierarchical porous network. Hyper polarized xenon NMR measurements demonstrated the connectivity between the resulting micro-and meso-pores. (p. 24)
- Simple solution-based blending of a homopolymer with a block co-polymer has been shown to direct the formation of a variety of ordered nanostructured phases. Such structure-directing properties were also seen upon addition of water or ionic salts to a block co-polymer. (p. 26)
- Chemical (pH and ionicity) and thermal stimuli are shown to produce reversible volume changes in hydrogels. Specifically, a Bragg reflector whose reflectivity varies with pore spacing produced by change in pH and the capture and release of proteins by heating and cooling, respectively, of a hydrogel have been demonstrated. (p. 28)
- Controlling the extent of the oxidation of the ferrocene moiety in the backbone of anionically synthesized poly (styrene-*block*-ferrocenyldimethylsilane) copolymers has provided a means for order formation and control over the microstructure of the polymer. (p. 30)

Nanoscale Phenomena in Perovskite Thin Films

Objective

Develop the scientific basis for controlling nucleation, growth and strain in ferroelectric perovskite thin films.

Highlights

- It has been demonstrated for the first time that 90° domains can move by the application of an electric field in ferroelectric thin films where the clamping of the film by the substrate is greatly reduced, or removed, by nanostructuring. The resulting switching of 90° domains leads to enhanced piezoelectric response. (p. 32)
- Precise control of Pb stoichiometry has been shown to be essential for the fabrication of thin films of high zirconia PLZT that have 2-4 times the energy density and much higher dielectric breakdown strength than current state-of-the-art materials. (p. 34)
- A comprehensive X-ray scattering study of PbTiO_3 thin films grown on SrTiO_3 substrates as a function of thickness in the nanoscale thickness regime has demonstrated that a minimum thickness of 3 unit cells is needed for the existence of ferroelectricity in this strained system. (p. 36)

The Science of Localized Corrosion

Objective

Advance the fundamental understanding of the mechanisms leading to the initiation, propagation and cessation of localized corrosion of aluminum and its alloys to permit accurate life predictions and intelligent designs.

Highlights

- TEM and SEM studies have provided the first observation of nanoscale voids within the passive oxide on aluminum under pre-pitting electrochemical conditions. The existence of these voids has been invoked in leading models of localized (pitting) corrosion. (p. 38)
- The first quantitative kinetics measurements of Al_2O_3 oxide film (on aluminum) dissolution in the presence of Cl^- ions have provided new insights into the chemical stability of the oxide film and localized corrosion. The rate of dissolution increases rapidly at sufficiently high Cl^- concentrations and tends towards a saturation value. (p. 40)
- Density functional theory calculations have provided new insights into the surface interactions at the copper-water interface and the reorganization of the nuclei in response changing electronic charge. The mechanism for hydrogen evolution under sufficiently high cathodic polarization is identified. (p. 42)
- *Ab initio* modeling via density functional theory has revealed the mechanism by which deprotonation and migration of adsorbing water upon copper (111) transitions into oxidative chemistry at the interface under anodic polarization. (p. 44)

Controlled Defect Structures in Rare-Earth-Ba-Cu-O Cuprate Superconductors

Objective

Provide an integrated scientific understanding of lattice defects and their nanoscale structure in the “123” rare-earth cuprates and related compounds, their dependence on the various methods of synthesis, and their relationship to the resulting superconducting properties.

Highlights

- A substantial data base on the influence of film thickness (d) on the critical current density (J_c) of YBCO coated conductors shows that this dependence is satisfactorily described by $J_c \propto 1/d^{1/2}$. While this relationship is predicted from a collective flux pinning model of randomly distributed point defects, film thinning studies suggest that the thickness dependence is primarily a materials effect associated with the liquid-mediated growth. (p. 46)
- The thickness dependence of the ac losses in disks of YBCO films in perpendicular magnetic fields reveals a very strong increase in loss with decreasing thickness at low fields. The results follow the predictions of two critical-current density models for thin ($0.2 \mu\text{m}$) and thick ($1.0 \mu\text{m}$) films. (p. 48)
- Two complementary on-line diagnostic techniques, reel-to-reel x-ray diffraction and reel-to-reel Raman microscopy, have been developed for the in-situ process monitoring and control of YBCO coated conductors. The capabilities of these techniques have been demonstrated. (p. 50)

Carbon-Based Nanostructured Materials

Objective

Advance the science and technology of carbon-based materials that will lead to the development of new generations of MEMS and NEMS devices.

Highlights

- Low-temperature (400°C) deposition of ultrananocrystalline diamond films with relatively high deposition rate (0.2 $\mu\text{m/hr}$) and low intrinsic stress has been achieved by using microwave plasma chemical vapor deposition (MPCVD). These films are expected to have excellent mechanical, chemical and tribological properties. (p. 52)
- Preliminary studies have shown that controlling the surface chemistry of ultrananocrystalline diamond films can result in large changes in nano-scale adhesion and probably friction as well. The results point the way toward strategies for optimizing this material for MEMS and NEMS applications. (p. 54)
- The effects of load on the friction and wear characteristics of a number of different diamond films, under various ambients and loads revealed a trend of increased friction with decreasing load - a result that has strong implications from MEMS devices. (p. 56)

Granular Flow and Kinetics

Objective

Develop constitutive relationships for the dynamic response of granular materials capturing the breadth of granular kinetics and flows in fundamental ways.

Highlights

- Electrostatic driving by applied electric fields in combination with high speed imaging are shown to allow precise and controlled characterization of the velocity statistics in driven granular media and of the formation and coarsening of granular ensembles. (p. 58)
- Simulations of hopper flow using a highly parallel molecular dynamics code on a large number of particles have provided realistic and precise information about the influence of various parameters on internal forces and flow. Some of this information cannot be obtained experimentally. (p. 60)
- A combination of experiments and theory/simulations has allowed the probing of the role of non-equilibrium (athermal) driving on the dynamics of granular polymers. It is shown that polymers driven out of equilibrium may be still accurately modeled by modifying existing equilibrium methods. (p. 62)

Experimental and Computational Lubrication at the Nanoscale

Objective

Develop a scientific understanding of lubrication and strategies to control tribology at the nanoscale capitalizing on recent advances in nanoprobe, theoretical and computational methods.

Highlights

- Molecular dynamics simulations have provided insight into the atomic-scale motion of self-assembled monolayers (SAMs), providing a picture of the molecular structure under shear and a detailed molecular-level understanding of energy dissipation mechanisms. (p. 64)
- New complementary experimental approaches have revealed structure and heterogeneous dynamics of confined fluid films that is more rich and complex than appears to have been anticipated by the current notions of “confinement-induced solidification”. Molecularly-thin fluid films constitute the essence of boundary-layer lubrication. (p. 66)
- A novel technique to control sliding friction at the nanoscale by applying external mechanical or electro-optical perturbations has been proposed. Two experimental setups to test the concept are being implemented. (p. 68)

Research Briefs

Interfacial Modification in Nanocomposite Permanent Magnets

J. S. Jiang, J. E. Pearson, and S. D. Bader, Argonne National Laboratory

J. P. Liu, University of Texas-Arlington

L. H. Lewis and D. C. Crew, Brookhaven National Laboratory

J. Kim and K. Barmak, Carnegie Mellon University

Motivation—*Exchange spring* nanocomposite permanent magnets provide a way to create the next generation of ultra-strong magnets with important energy implications. These magnets are promising because they fully exploit the favorable properties of each constituent phase to produce a magnet superior to either of its components. The performance of an exchange spring system is controlled by the exchange coupling between the constituent phases and their intrinsic magnetic properties, and by the practical limits on controlling particle size and morphology during processing. Motivated by discussions that took place during the course of this CSP project, interfacial modification experiments were carried out in two model exchange-spring bilayer systems. The resulting changes in the magnetization behavior were compared and contrasted in order to define the conditions that foster the most robust interphase coupling in permanent magnets based on the exchange-spring principle.

Accomplishment—The strategy of modifying the structure-magnetism relationships in thin film bilayer systems by thermal annealing was the same in both sets of experiments. The systems chosen for study consisted in one case of chemically-ordered L1₀-type CoPt and Co bilayers, and in the other an epitaxial Sm-Co/Fe bilayers, where the epitaxy creates a well-defined magnetic anisotropy in the Sm-Co hard layer. The magnetic and microstructural properties were examined for bilayers of varying thicknesses and annealing conditions. Full exchange coupling of the soft magnetic layers to the hard

magnetic layers was not achieved in either case in the as-deposited state, as the major hysteresis loops displayed two-phase demagnetization behavior. Annealing caused the magnetic properties of the bilayers of both systems to resemble a more robustly coupled magnetic system. The CoPt/Co system exhibited a decreased remanence ratio and a single-phase demagnetization behavior upon annealing. Microstructure and phase determination verified that interdiffusion of the CoPt and Co layers occurred, with Pt diffusing into the soft Co layer to create a phase of intermediate anisotropy. On the other hand, annealing the Sm-Co/Fe system also made the hysteresis loop more single-phase-like, but without sacrificing the remanence ratio or the reversibility. X-ray reflectivity measurements indicated a smoothing of the Sm-Co/Fe interface and suggested the formation of a graded interfacial region where the material parameters vary continuously due to interdiffusion. In both cases, micromagnetic modeling demonstrated that alteration of the anisotropy profile could lead to changes in the magnetic behavior similar to those observed in the experimental studies.

Significance—The condition of the hard/soft interface in exchange-spring permanent magnets is of paramount importance. The results of this study help identify a potential pathway for developing a new generation of nanocomposite magnet materials. It is quite significant that both systems are forgiving of interfacial mixing and that it can actually lead to property improvements.

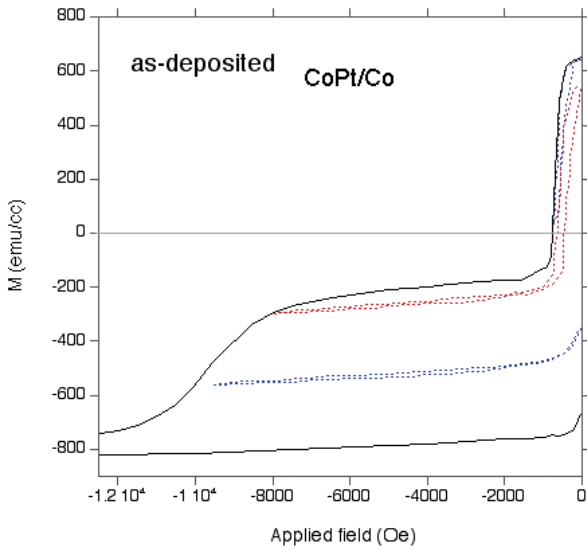


Figure 1a. Two-stage demagnetization curve and recoil loops of the CoPt/Co bilayer film in the as-deposited state.

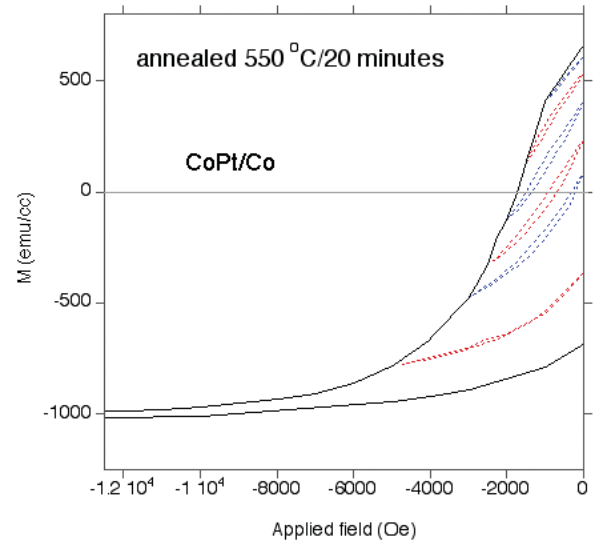


Figure 1b. Single-stage demagnetization curve and recoil loops of the CoPt/Co bilayer film after annealing at 550°C. Note this annealing treatment caused interdiffusion of the CoPt and the Co layer to produce a sandwiched layer of intermediate anisotropy.

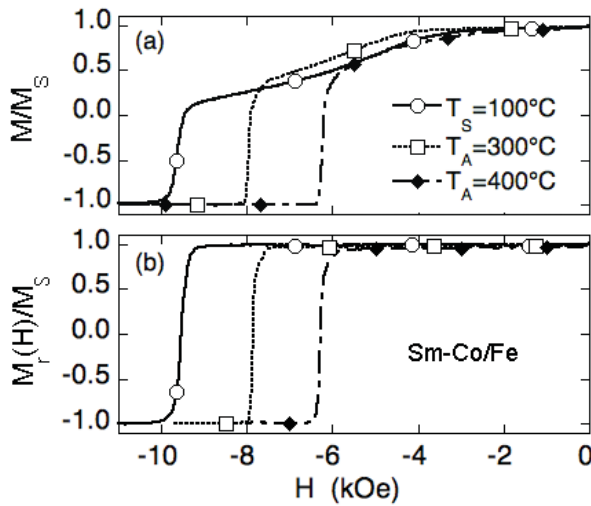


Figure 2 (a). Demagnetization and (b) dc demagnetization remanence curves for Sm-Co(200Å)/Fe(100Å) samples annealed at various temperatures.

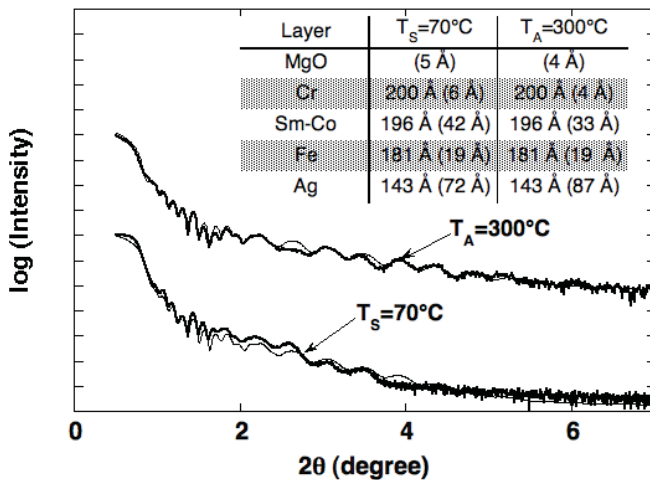


Figure 3. Measured (thick line) and fitted (thin line) x-ray reflectivity curves of as-deposited ($T_S=70^\circ\text{C}$) and annealed ($T_A=300^\circ\text{C}$) Sm-Co/Fe samples. The fitted layer thickness and roughness values (in parenthesis) are listed in the table for each layer.

Epitaxy and Residual Stress Induced Changes on the Curie Temperature of $\text{Nd}_2\text{Fe}_{14}\text{B}$

*M. J. Kramer, N. Yang, Y. Xu, K. W. Dennis and R. W. McCallum, Ames Laboratory
L. H. Lewis and D. O. Welch, Brookhaven National Laboratory
Y. Zhang and P. L. Lee, Argonne National Laboratory*

Motivation—Isotropic permanent magnets with enhanced magnetic properties can be obtained from a two-phase microstructure containing both hard and soft magnetic phases when the grain size of the soft phase is of order of the domain wall width in the hard phase. (Fig. 1). At these length scales, large intergranular stresses can be produced by the differences in the coefficients of thermal expansion and magnetostriction for the two phases. These stresses can be particularly large if there is strong elastic coupling along the interfaces between the different phases. In rare-earth (R) nanocomposite permanent magnets based on the $\text{R}_2\text{Fe}_{14}\text{B}$ (2-14-1) crystal structure, we have shown that there is a strong epitaxy of the Fe [110] lattice planes to the 2-14-1 [006] and 2-14-1 [330] lattice planes, as illustrated in Fig. 1. In this case the interfacial stresses can be on the order of ~ 400 MPa. Since the Curie temperature (T_c) of the 2-14-1 compound has a large pressure dependence of -26.5 K/GPa (J. Kamarad, *J. Magn. Magn. Mater.* **67** 29 (1987)) these stresses may be expected to have a measurable effect on T_c .

Accomplishment—To measure the effect of interfacial stresses on the T_c of $\text{Nd}_2\text{Fe}_{14}\text{B}$, careful lattice parameter measurements were performed as a function of temperature using high energy synchrotron x-ray diffraction at the Advance Photon Source, using the Ames Laboratory high temperature furnace. The lattice parameters of both the $\text{Nd}_2\text{Fe}_{14}\text{B}$ main phase and the Fe minor phase were determined for two different microstructures prepared by annealing aliquots of primarily amorphous melt-spun ribbon for 15 minutes at two different temperatures (923 K and 1173 K). Determination of the lattice parameters and refinement of the atomic positions for a high density of data points

in the vicinity of T_c has provided new and unexpected information about the interphase relationships in isotropic magnetic nanocomposites.

A comparison of the lattice parameters of the annealed ribbon samples shows that there is indeed a significant change in the 2-14-1 lattice parameters between the two annealing states. For example, the α -Fe (110) d-spacing in the optimized material tracks the 2-14-1 (006) d-spacing to $T = 450$ K (Fig. 2). This result is inconsistent with the normal temperature dependence of the lattice parameters for bulk α -Fe and indicates that the lattices of the two materials are strongly coupled at the atomic level. In addition, the thermal expansion coefficient of α -Fe was not linear as anticipated, but showed an inflection at the T_c of the 2-14-1 phase. The coincidence of the 2-14-1 and α -Fe thermal behavior is attributed to the large surface-to-volume ratio present in the nanocomposites which is substantially reduced with the higher temperature anneal, yielding a coarser microstructure. Using the α -Fe lattice as an internal piezometer, it is possible to calculate the internal stresses due to the combined effect of the differences in the coefficients of thermal expansion and the effect of the large magnetostriction of the 2-14-1 (Fig. 3). The solid line is the measured thermal expansion for bulk α -Fe. These stress values result in reasonable changes of ~ 5 K in the $\text{Nd}_2\text{Fe}_{14}\text{B}$ T_c based on its known pressure dependence.

Significance—The observed strong epitaxy between the (006) planes of the 2-14-1 lattice and the (110) planes of the α -Fe results in large intergranular stresses in both materials. These stresses can have a significant influence on magnetic properties.

Contact: Matthew J. Kramer, Ames Laboratory
Phone: (515) 294-0276, Fax: (515) 294-4291, E-mail: mjkramer@ameslab.gov

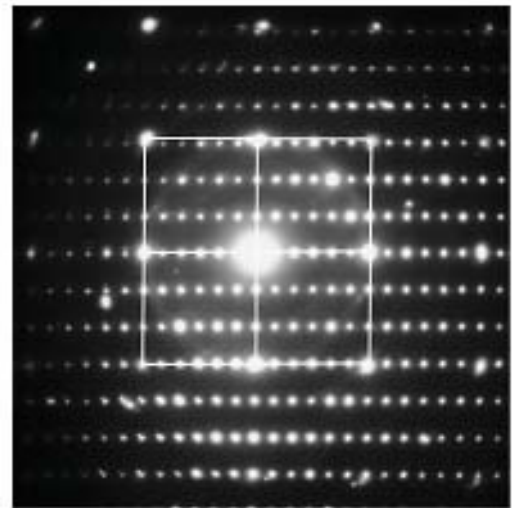
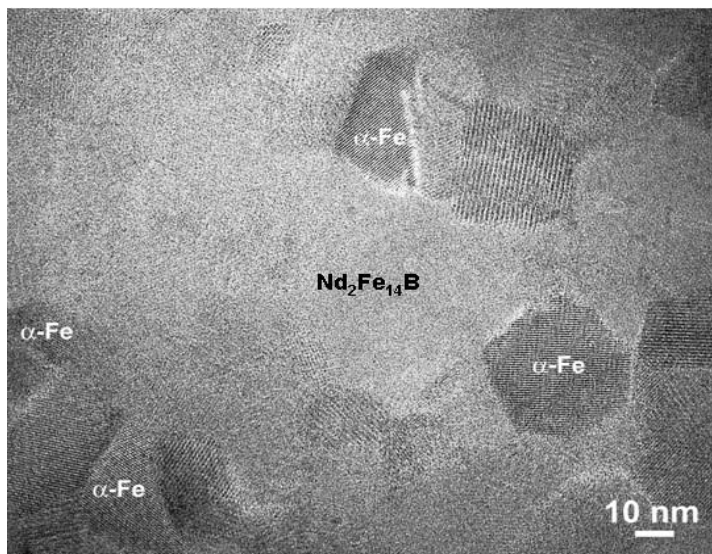


Figure 1. TEM micrograph (left) showing the typical structure of melt-spun exchanged-coupled nanocomposite of α -Fe and $\text{Nd}_2\text{Fe}_{14}\text{B}$. Selected area diffraction pattern (right) showing epitaxy between 2-14-1 and α -Fe, outlined in white.

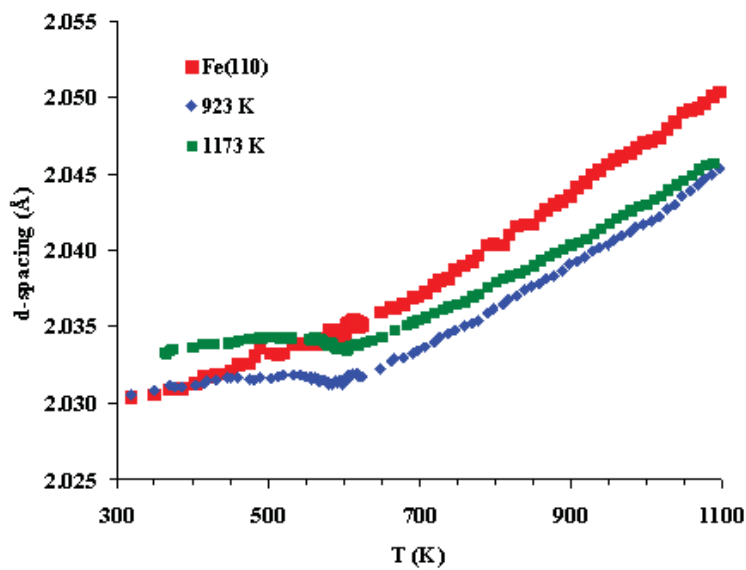


Figure 2. Comparison of the temperature evolution of 2-14-1(006) d-spacing for two different annealing temperatures (blue, 923 K and green, 1173 K) of $\text{Nd}_2\text{Fe}_{14}\text{B}$ and the corresponding α -Fe₍₁₁₀₎ d-spacing (red), in the melt-spun nanocomposite materials. Note that the d-spacings of the 2-14-1 and α -Fe track up to 450 K and that the Curie temperature is less for the lower temperature anneal.

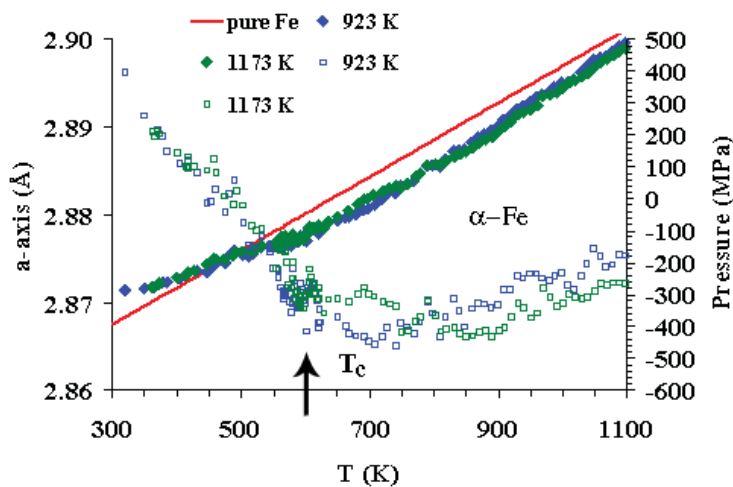


Figure 3. Piezometry: Comparison of the d-spacing of α -Fe in the nanocomposite material (closed symbols) with that of unstressed, pure α -Fe, as a function of temperature. The α -Fe phase in the nanocomposite is under tension at room temperature but becomes compressive due to the magnetostriction of the $\text{Nd}_2\text{Fe}_{14}\text{B}$ phase at its Curie point (arrow). Annealing coarsens the nanostructure and reduces the compressive stresses.

Ferro-/Antiferro-Magnetic Competition in FePt Alloys

G. Brown, Florida State University

B. Kraczek and D. D. Johnson, University of Illinois Urbana

A. Jonotti, T. C. Schulthess, and G. M. Stocks, Oak Ridge National Laboratory

Motivation—High-density magnetic recording has been undergoing rapid refinement with information now stored in bits with dimensions approaching 10 nm. These advances have placed stringent requirements on the recording media. For instance, maintaining the thermal stability of information recorded in these small volumes requires high magneto-crystalline anisotropy energy (MAE). A candidate material for satisfying this necessary requirement is the ordered intermetallic alloy FePt. Interest in FePt has been heightened by the recent discovery of a chemical pathway in which mono-dispersed FePt particles with tunable diameters from 3 to 10 nm can be synthesized. Understanding the nature of the magnetism in these particles is important for their potential use in recording media and, more generally, in nanocomposite magnets. The present first-principles calculations are a step towards this objective.

Accomplishment—Motivated by these considerations, and previous success with modeling Fe nanoparticles and nanowires using spin Hamiltonians, we initiated work to generate a first principles based spin model for FePt nanoparticles and nanowires. Although the calculated interactions were obtained based on an assumed ferromagnetic ground state for FePt (which is what is found experimentally) the interactions indicated a possible antiferromagnetic (AFM) ground state. Subsequent first principles calculations for the AFM state

(up/down ordering of alternate Fe- planes of the $L1_0$ structure) revealed that AFM is indeed the ground state. More extensive calculations using various first principles methods confirm the AFM state but also indicate a near degeneracy between the ferromagnetic and AFM states, with energy differences less than room-temperature thermal energy. Why then is FePt found, experimentally, to be ferromagnetic?

Consideration of the effects of the long-range order (LRO) parameter (η) on the magnetic state show that the ferromagnetic -(FM) state is stabilized by anti-site defects (disorder) - see Fig 2. This result opens up the possibility that it may be difficult to experimentally produce FePt in an ideal LRO-ed state. A conjecture that now needs to be checked via experimental X-ray scattering studies is the effects of temperature and processing on the LRO parameter. Additionally, consideration of the effects of tetragonality reveals that the FM-state is destabilized as the tetragonal distortion is decreased towards the ideal c/a ratio of unity (Fig. 1).

Significance—Taken in combination, these findings offer interesting avenues for experimental investigation in that it may be possible to tailor the properties of FePt, *i.e.* maintain both the FM state and the high MAE (generally MAE decreases with decreasing η), through the simultaneous control of η and c/a through processing and additional alloying.

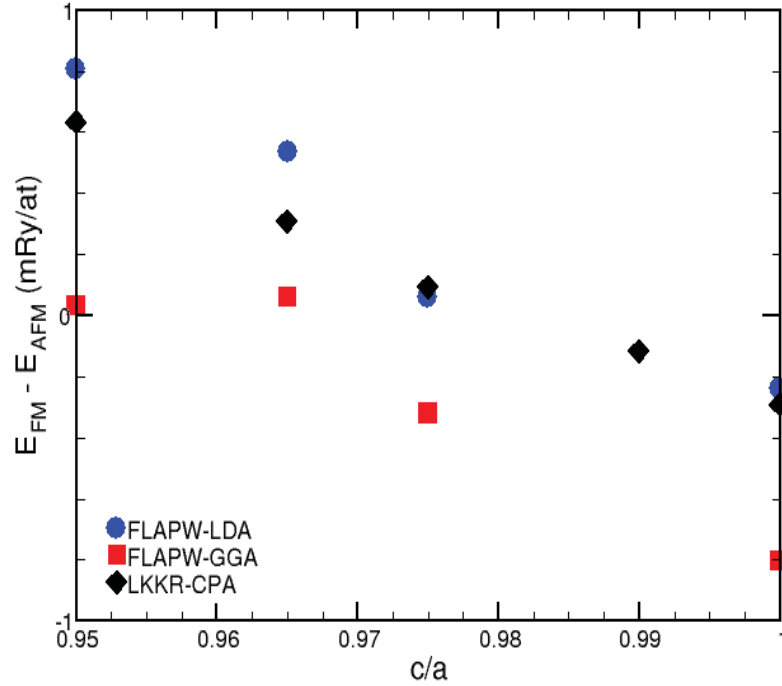


Figure 1. Total-energy differences between ferromagnetic, E_{FM} , and antiferromagnetic, E_{AFM} , states vs. c/a . The ferromagnetic state is more favorable as $c/a \rightarrow 1$. The antiferromagnetic state is more favorable for non-ideal c/a . All results are for perfectly ordered L1_0 FePt with $\eta=1$, *i.e.*, in the absence of chemical disorder. Calculations were performed using the local density approximation (LDA) as well as the Generalized Gradient Approximation (GGA) to density functional theory.

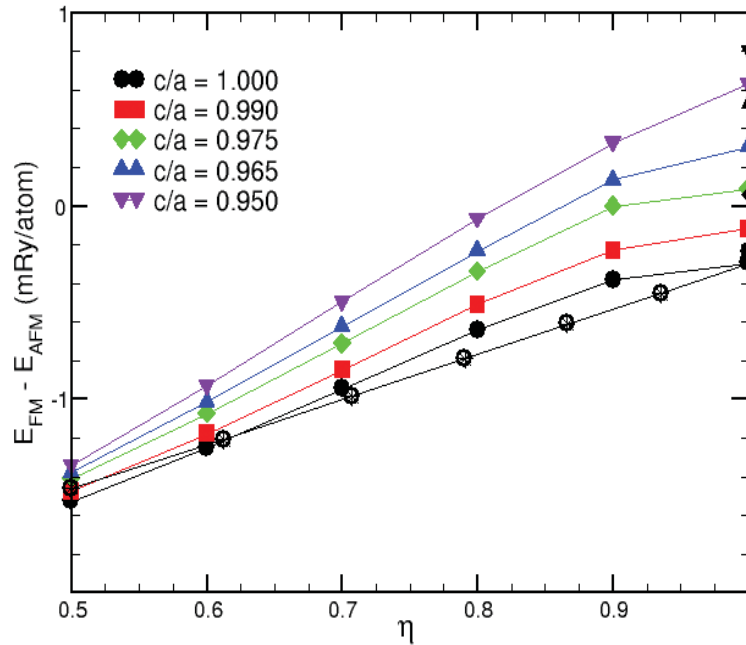


Figure 2. Total-energy differences between ferromagnetic, E_{FM} , and antiferromagnetic, E_{AFM} , states vs. the long-range order parameter η for LKKR-CPA (open symbols) and bulk KKR-CPA (star-filled symbols). Several c/a (R) values with fixed unit-cell volume are used. The solid lines are a guide-to-the-eye. The solid symbols are FLAPW-LSDA results.

Approaches to Self-Assembled Nanoscale Materials with High Porosity

T. Baumann and G. Fox, Livermore National Laboratory

G. Long, M. Smith, and J. Mercer-Smith, Los Alamos National Laboratory

L-Q Wang and Y. Shin, Pacific Northwest National Laboratory

I. L. Moudrakovski, Steacie Institute for Molecular Sciences, NRC, Canada

Motivation—Materials with high porosity are used as catalysts, as waste sequestration agents, as low dielectric constant layers for IC applications and in many other technical areas. While it is relatively easy to impart porosity into a ceramic or polymer network, the low mechanical strength of the resulting material can preclude its use for many of these applications. A ball-and-stick model synthesis approach is but one method to improve the strength of these highly porous but mechanically fragile materials. The idea is to introduce at least two levels of porosity: (1) microporosity within the porous "ball" structures; and, mesoporosity within the rigid stick framework. To characterize porosity size and interconnectedness on the molecular level, a new magnetic resonance approach has been developed. Results can be used to modify processing conditions in order to achieve targeted porosity and increased mechanical strength.

Accomplishment—A scheme for preparing these materials is illustrated in Figure 1. Here, a dendrimer core (organic aerogel) is combined with a rigid rod spacer to form the hierarchical porous network. The core is based upon a resorcinol-formaldehyde resin that is formed upon addition of a catalyst to the precursor mixture.

The porosity size, size distribution, and network interconnectedness within the dendrimer core is probed by means of hyper polarized xenon NMR measurements as seen in Figure 2. This sensitive measurement is an analog of the temperature programmed desorption technique used to probe molecular affinity to surfaces. The 2D chemical exchange ^{129}Xe NMR illustrates that narrow and broad signals are associated with mesopore and micropore regions, respectively. The exchange between the mesopore and micropore is faster than between two micropores, indicating micropore connectivity to the mesopores (Figure 3).

Significance—Modification of co-assembly routes to the preparation of rigid polymer structures with hierarchical interconnected porosity is driven by magnetic resonance measurements that probe the resident pore structure in these materials. In addition to the application areas described above, use of these materials as Internal Confinement Fusion (ICF) targets is likely. The ability to tailor the x-ray opacity and density of foams would give greater flexibility in the design of targets and enable fine resolution studies of hydrodynamic instabilities.

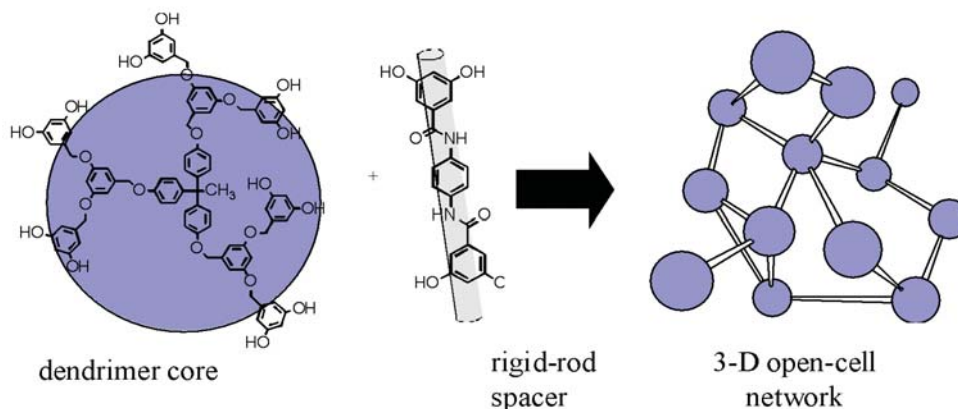


Figure 1. General scheme for engineering rigid, porous networks.

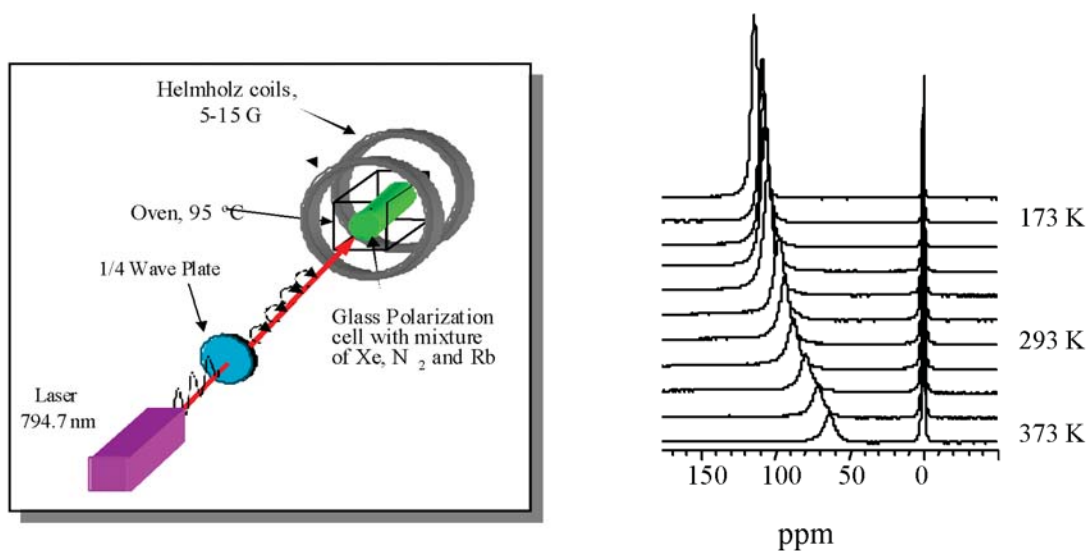


Figure 2. Hyper polarized ^{129}Xe NMR Spectroscopy - Spin polarized xenon vapor percolates through the interconnected nanoporosity; the ^{129}Xe line exhibits a chemical shift and broadening that changes with the size and chemical nature of the pores.

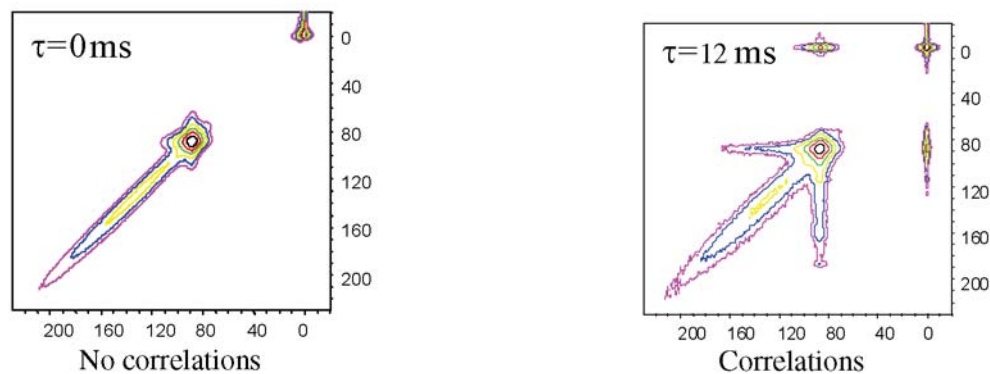


Figure 3. 2D CF ^{129}Xe NMR in RF Aerogels is taken to resolve the origin of the signals in the spectra of adsorbed Xe and to evaluate interconnectivity between different adsorption regions. The exchange between regions of different chemical shift manifests itself in the appearance of the cross-peaks between signals from the exchange sites.

Induced Ordering Phenomena in Block Co-Polymer Systems

H-H. Wang, Argonne National Laboratory

J. McBreen, Brookhaven National Laboratory

T. Habenschuss, Oak Ridge National Laboratory

G. J. Exarhos and Y. Shin, Pacific Northwest National Laboratory

Motivation—Co-polymer systems consisting of both hydrophilic and hydrophobic units will spontaneously self-order based upon the magnitude of localized inter- and intra-molecular interactions among the constituent blocks. This ordering also can be induced by addition of a homopolymer phase, a hydrophilic liquid such as water, or even an ionic salt phase. The intrinsic chemistry of the added specie will influence these interactions and subsequently stabilize a targeted ordered structure. Selective removal of the phase modifier will leave the overall structure intact but will induce porosity at the nanoscale and concomitant high surface area making these materials quite useful as sequestration agents, gas filtration membranes, and improved ionic conductors for battery applications.

Accomplishment—A homopolymer was blended with a block co-polymer and allowed to relax into a self-organized phase. The chemical nature and amount of homopolymer addition were found to influence the resulting ordered phase as seen in Figure 1. Such structure directing properties were also seen upon addition of water or ionic salts. Perturbations to the structure caused by these additions were evaluated by

electron microscopy, small angle x-ray and neutron scattering measurements, and atomic force microscopy (AFM). Selective etching of two phases from a gyroid phase material produced the unique microstructure also shown in Figure 1.

The effect of water addition to a block co-polymer in tetrahydrofuran solvent is shown in Figure 2. Above a critical water content, the individual polymer fibers assemble into nanofiber bundles that can be imaged in solution by means of fluorescence microscopy. Upon solvent evaporation on a mica substrate, the 18 nm diameter fibrils form an aligned microstructure as determined by both AFM and small angle neutron scattering.

Significance—Simple solution-based mixing approaches to the formation of ordered nanostructured phases provide a "bottoms-up" processing alternative to the formation of these intricate structures. Control of the ordered and interconnected porosity is enabling to producing new materials with applications to high current carrying electrolytes for batteries, biocatalysis for pharmaceutical production, and waste sequestration.

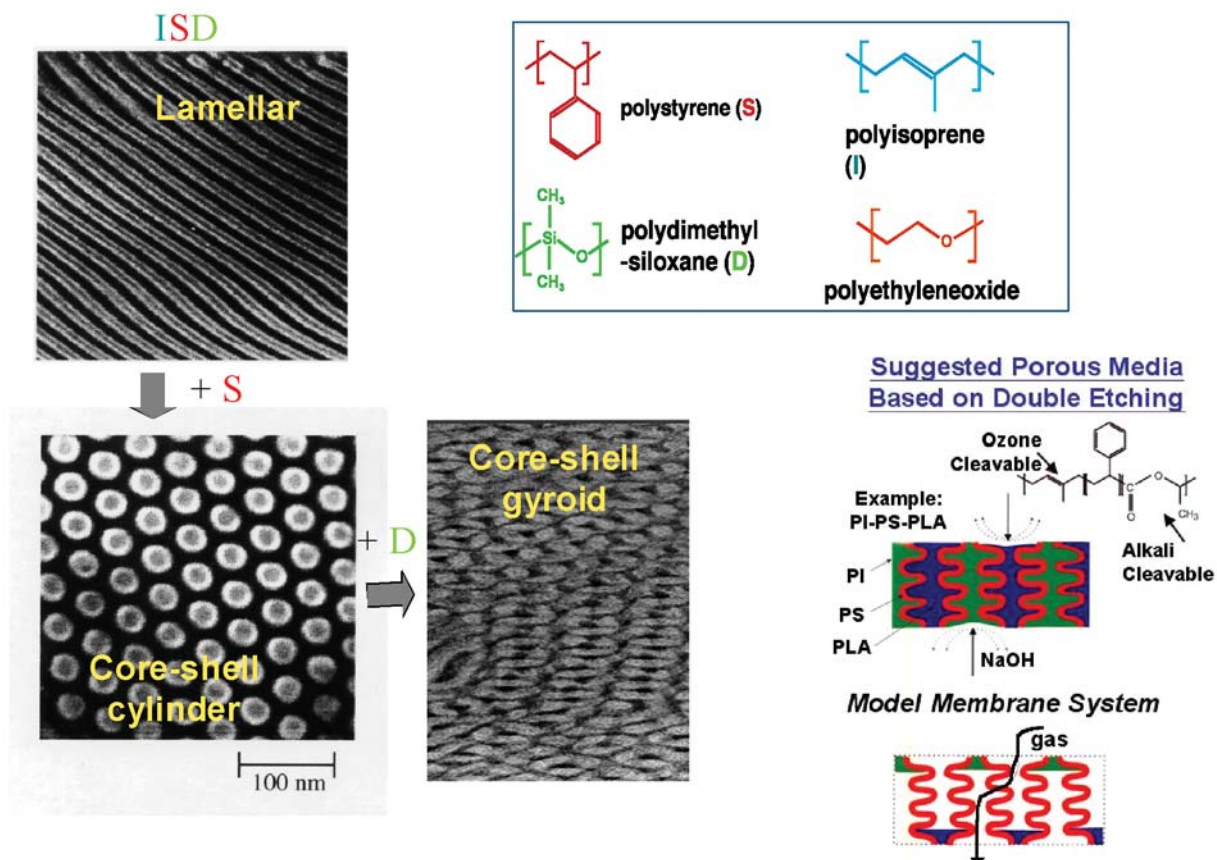


Figure 1. Homopolymer addition to a block copolymer directs formation of ordered nanostructures and promotes transformation between these structures. Shown at the lower right is a gas separation membrane based on double etching of the gyroid phase.

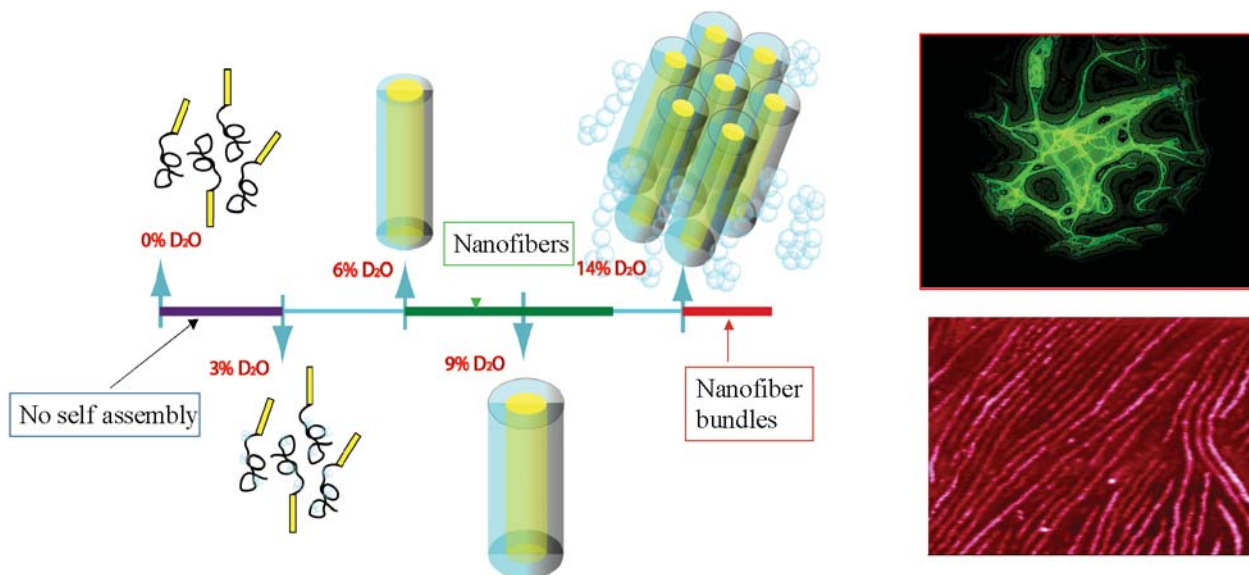


Figure 2. Effect of D₂O addition on structural ordering in polyglycol/polyvinylidene co-polymer showing microfibril formation and fluorescence microimages.

Hydrogel-Water Interactions for Sensing and Controlled Release

P. V. Braun, University of Illinois/F5-MRL

B. C. Bunker and D. L. Huber, Sandia National Laboratories, NM

Y. Shin, Pacific Northwest National Laboratory

Motivation—Hydrogels are an amazing class of polymers that respond reversibly to ambient changes in the local solution environment. For example, raising the temperature can induce a loosely packed arrangement of molecules to transform into a compacted layer with concomitant large decrease in volume. At constant temperature, changes in solution pH or solution salt loading also will promote a reversible volume change. These properties are most useful for the design of robust sensors and controlled release surfaces. By creating ordered porosity in a material with spacing on the order of visible light wavelengths, the material also will serve as a variable Bragg reflector that changes color commensurate with the volume change. Surface bound hydrogels can be utilized for controlled adsorption and release of proteins by taking advantage of the changing hydrophilicity of the surface.

Accomplishment—The bicontinuous pH-sensitive inverse opal hydrogel with stimuli-sensitive optical response was synthesized by means of a colloidal crystal templating process. A mixture of 2-hydroxy-ethyl methacrylate (HEMA) and acrylic acid (AA) comprised the system of interest owing to both chemical and mechanical robustness. The resulting interconnected pore network allows ready diffusion of solution

throughout the structure thereby improving the response of the network to the ambient environment (Fig. 1). A colloidal template with characteristic spacing on the order of several hundred nanometers was used to fix the hydrogel thereby creating a Bragg reflector whose optical properties vary with pore spacing which in turn depends upon solution pH and solution ionicity. Figure 2 shows schematics of a reflection measurement and measured data as the hydrogel is exposed to different pH environments.

The hydrogel based upon poly(N-isopropylacrylamide), PNIPAM, undergoes a reversible volume change near 30°C. At higher temperatures, intermolecular hydrogen bonding breaks down leading to collapse of the network and producing a hydrophobic, protein adsorbing surface. Protein molecules bound to this surface will be released upon cooling (Fig. 3).

Significance—The fabrication of smart materials that respond reversibly to changes in their ambient environment is based upon second order phase transformations induced thermally or by chemical stimuli such as pH or solution salt content. Such materials have applications in the sensor arena and in the biopharmaceutical industry where controlled release from a surface is required for drug delivery.

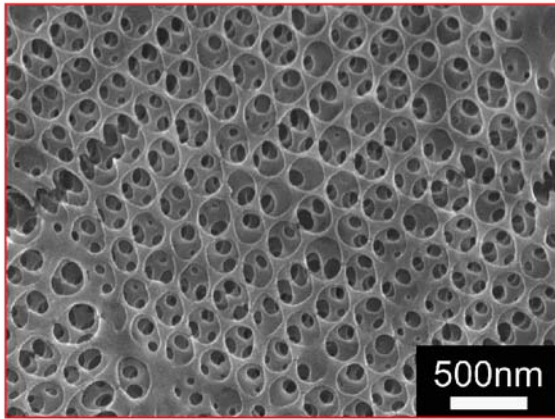


Figure 1. Colloidal crystal templated hydrogel showing the interconnected porous microstructure.

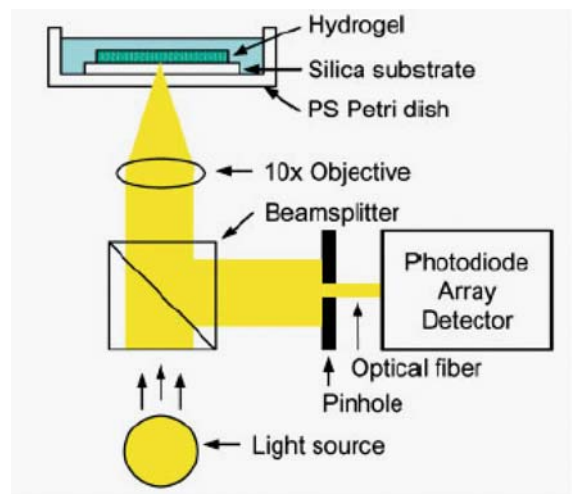
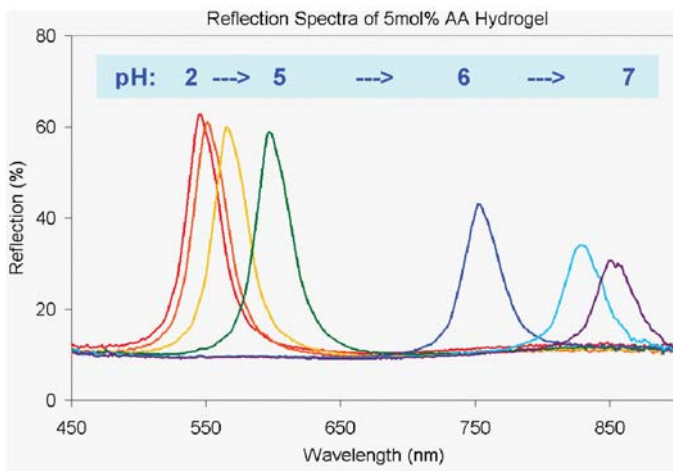


Figure 2. Schematic of the optical reflection measurement and measured reflectance spectra from the hydrogel as a function of pH.

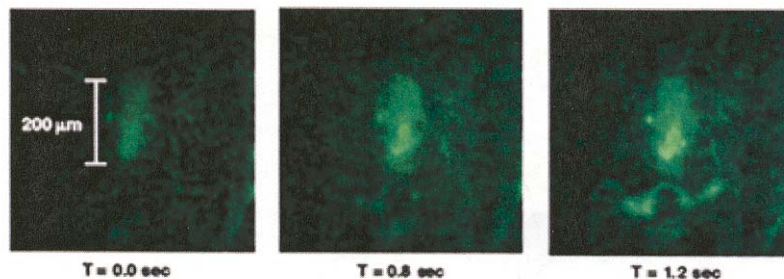


Figure 3. Fluorescence microscopy images of fluorescein-labeled myoglobin (green) interacting with a PNIPAM coated micro-heater line. Left - Image obtained on heating a line above the PNIPAM transition temperature after exposure to a 0.5 mg/ml myoglobin solution. Right - Images obtained 0.8 and 1.2 seconds after the hot line was turned off, releasing a plume of protein into a stagnant solution.

Characterization of Electrochemically-Active Block Copolymers

H. B. Eitouni and N. P. Balsara,
Lawrence Berkeley National Laboratory

Motivation—Diblock copolymers, because of their ability to self assemble into interesting and useful morphologies, have received much attention for use as lithographic materials, photonic crystals, filters, and many other applications [1]. These applications require organizing inorganic domains within block copolymers, and the success of such projects hinges on the development of a fundamental understanding of the interactions between organic and inorganic materials. Our work is based on the pioneering studies of Manners and coworkers who demonstrated methods for synthesizing block copolymers with an organometallic poly(ferrocenylsilane) block [2]. These materials are particularly interesting due to the redox activity of the ferrocene moieties as well as their interesting chemical and physical properties. Poly(ferrocenylsilane)s, composed of alternating ferrocene and dialkylsilane units in the main chain, show electrostatic interactions between neighboring iron atoms in the charged state. Intra- and inter-molecular interactions in these systems can thus be adjusted electrochemically or by the addition of charged species, thereby providing additional means to control order formation.

Accomplishment—The thermodynamic interactions in anionically synthesized poly(styrene-*block*-ferrocenyldimethylsilane) (SF) copolymers were examined using small angle X-ray scattering (SAXS). The temperature dependence of the Flory-Huggins parameter, χ of SF copolymers, determined by SAXS, is similar in magnitude to that between polystyrene and polyisoprene chains, a typical organic block copolymer. We find that χ is independent of block copolymer composition as predicted by the Flory-Huggins theory. Figure 1 shows χ as a function of T for two SF copolymers [3].

The thermodynamic interactions in SF copolymers were systematically adjusted by oxidation of the ferrocene moiety with silver nitrate and examined using SAXS. The polymer retained a microphase separated ordered structure upon oxidation and showed a systematic change in the location of the order-disorder transition as a function of ferrocenium nitrate content. Figure 2(a) shows the dependence of the order-disorder transition temperature on the percent oxidation of the ferrocene for a specific SF diblock copolymer. A partially oxidized SF block copolymer is shown in Figure 2(b). Two platinum electrodes have been inserted in the sealed sample between quartz windows. By applying a potential across the system, we have caused a concentration gradient of ferrocenium nitrate to develop. The red region in the sample is the SF copolymer after it has been reduced back to its original state. By controlling the extent of oxidation of ferrocene to ferrocenium, we may be able to control order formation of the diblock copolymer.

Significance—By controlling the redox properties of the ferrocene moiety in the backbone of the polymer, we have provided a method for control over microstructure not yet explored. By combining this procedure with electrochemical techniques, we may develop a novel method of controlling the order-disorder transition of organometallic block copolymers and their bulk properties.

1. Park, M.; Harrison, C.; Chaikin, P. M.; Register, R. A.; Adamson, D. H. *Science* **1997**, 276, 1401
2. Rulkens, R.; Lough, A.J.; Manners, I. *J. Am. Chem. Soc.* **1994**, 116, 797.
3. Eitouni, H. B.; Balsara, N. P.; Hahn, H.; Pople, J. A.; Hempenius, M. A. *Macromolecules* **2002**, 35, 7765.

Contact: N. P. Balsara, Lawrence Berkeley National Laboratory
Phone: (510) 642-8973, Fax: (510) 642-4778, E-mail: NPBalsara@lbl.gov

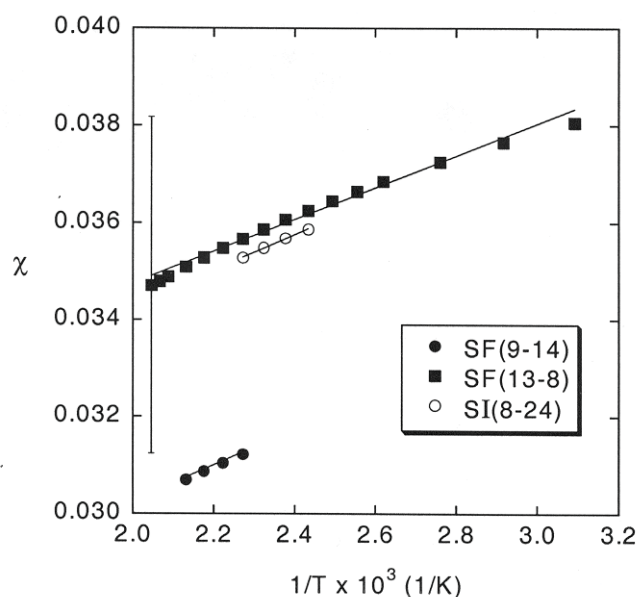


Figure 1. Flory-Huggins interaction parameters χ between poly(ferrocenyldimethylsilane) and polystyrene based on analysis of the SAXS data, assuming a single statistical length for both blocks. The numbers in parentheses refer to the molecular weights of the respective blocks in kg/mol. Data for a poly(styrene-*block*-isoprene) sample has been included for comparison. The reference volume is 100 \AA^3 . Error bar represents average uncertainty. Note the highly expanded ordinate scale.

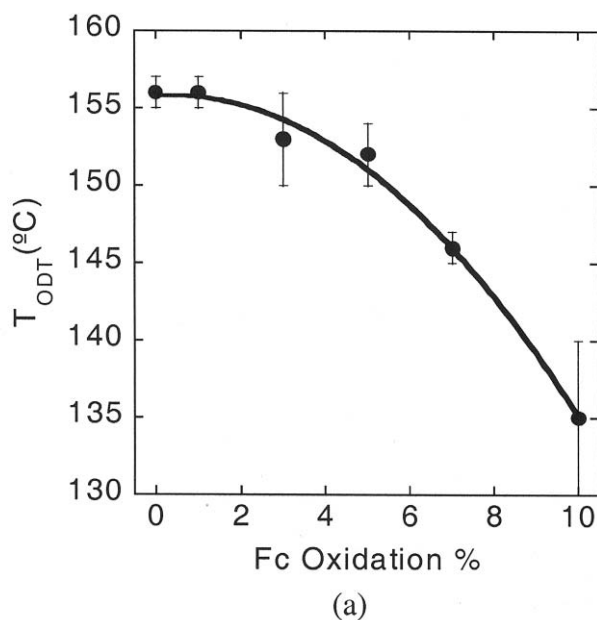


Figure 2. (a) The order-disorder transition temperature of SF(9-14) as a function of the amount of oxidation of the ferrocene in the system. Oxidation was performed using AgNO_3 in dichloromethane. T_{ODT} was determined from SAXS peak width analysis. (b) An electrochemical cell containing a partially oxidized SF block copolymer dissolved in dichloromethane. Red regions are ferrocene rich and darker regions are ferrocenium nitrate rich.

Limit of Ferroelectricity in Ultra-Thin Perovskite PbTiO_3 Films Identified by In Situ Synchrotron X-ray Scattering Studies

G. B. Stephenson, O. Auciello, J. A. Eastman, D. D. Fong, P. H. Fuoss, and S. K. Streiffer,
Argonne National Laboratory

C. Thompson, *Northern Illinois University and Argonne National Laboratory*

Motivation—Complex Oxide piezoelectric and ferroelectric thin films are used or envisioned for numerous diverse applications such as sensors, actuators, and non-volatile memories. Although stripe domains have long been expected to occur in ferroelectric thin films and are postulated to affect their properties dramatically, there has been no direct evidence of their formation before this work. The observation of stripe phase can provide an excellent example of how novel ordered ground states may arise from chemically-induced, substrate-induced, or field-induced interactions in complex materials. Competition between these different interactions can be exploited to yield instabilities that enhance the sensitivity of the local atomic and electronic structure to a stimulus field. The ability to monitor structure *in situ* during thin film processing is also critical for property optimization.

Accomplishment—Using a unique *in situ* metalorganic chemical vapor deposition facility that we have integrated with a beam line at the BESSRC Sector 12-ID of the Advanced Photon Source, we have investigated the growth and properties of the prototypical perovskite PbTiO_3 (PTO), synthesized as thin films with thicknesses from 1 unit cell to 100 unit cells. We have experimentally demonstrated for the first time that epitaxially-strained PbTiO_3 grown on SrTiO_3 exists in a non-centrosymmetric (ferroelectric) tetragonal phase as much as 200°C above the bulk ferroelectric-to-paraelectric phase transition temperature, approaching the theoretically predicted value of 752°C (Pertsev *et al.*, PRL, **84**, 3722, 2000) for film thicknesses

of approximately 100 unit cells. However, the phase transition temperature is observed to decrease with decreasing film thickness, as expected if the polarization at the interfaces is intrinsically suppressed relative to its equilibrium value in the bulk. Data from the x-ray scattering experiments also show for the first time that depolarization-induced 180° stripe domains form in ferroelectric thin films, as evidenced by evolution of distinctive satellite features around PbTiO_3 Bragg peaks [see Fig. 1 (a) and (b)]. These studies demonstrated that 3 unit cells seem to be the lower limit of PTO film thickness for the existence of ferroelectricity [see Fig 2]. By analyzing the variation of stripe period with film thickness, we have been able to extract the 180° domain wall energy. Cooling samples to room temperature results in a second structural transition from this striped structure to the commonly observed ferroelastically-distorted microstructure consisting of non-ordered c-axis oriented domains and a small volume fraction of 90° domains (twins).

Significance—Our rapidly increasing ability to tailor three-dimensional nanostructures offers the promise of developing new ways to control and utilize novel ground states as well. The present work demonstrates that nanostructuring via thin film processing has the potential for controlling and significantly enhancing ferroelectric performance. Most importantly for the field of ferroelectric films, our data provide one of the first truly comprehensive investigations of ferroelectric film properties as a function of thickness and temperature in the nanoscale thickness regime.

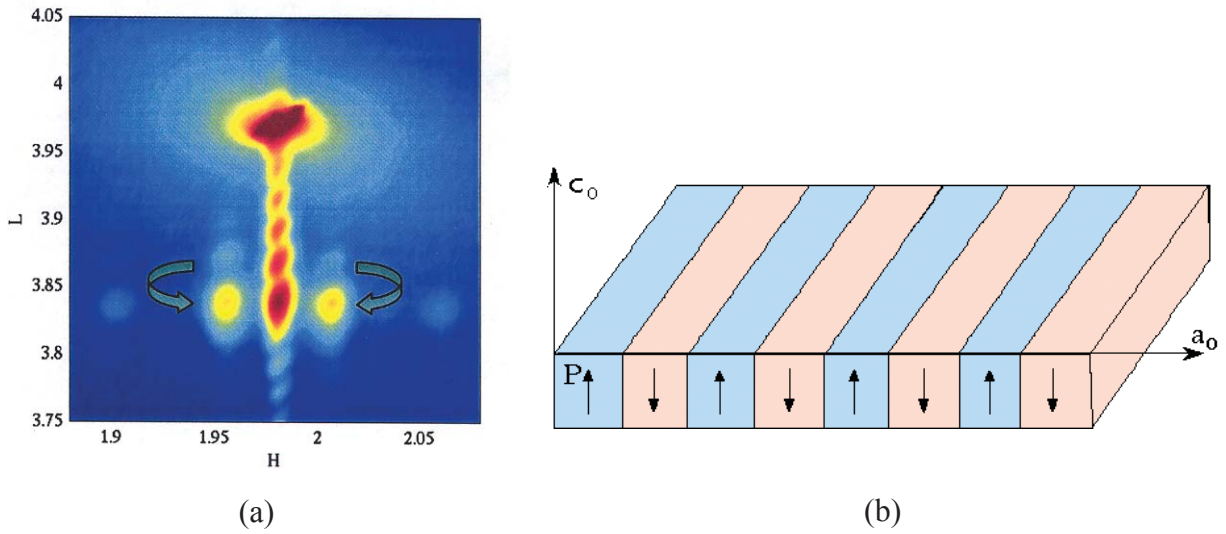


Figure 1. (a) superlattice modulations (arrowed) appear around the PbTiO_3 Bragg peak in the spectrum of x-rays scattered from epitaxial PbTiO_3 films grown on single crystal STO substrates. The scattering modulations arise from highly periodic 180° polarization stripes generated in the film as shown in the schematic in (b).

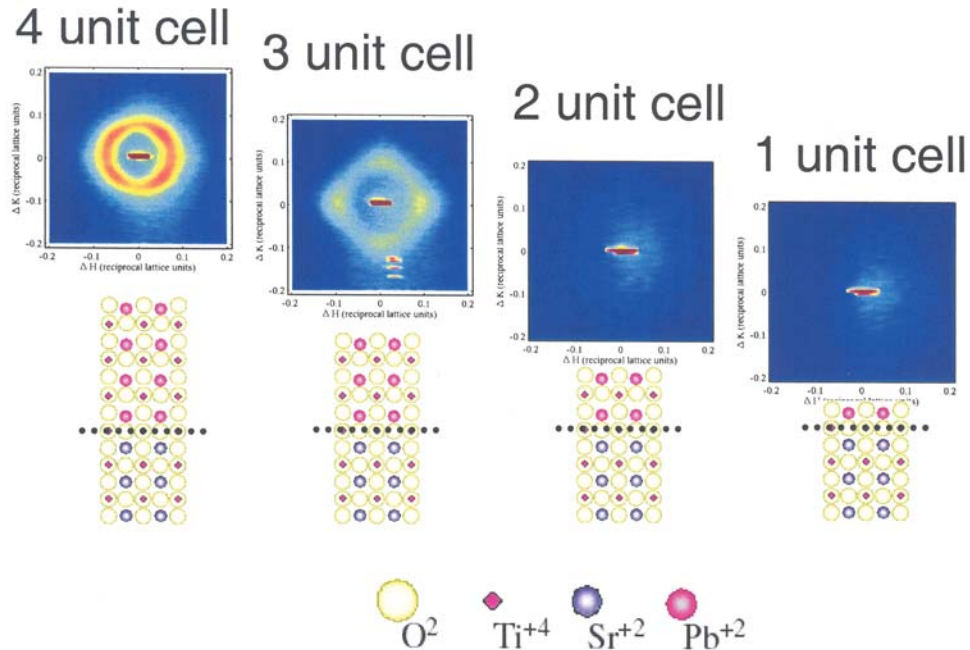


Figure 2. In situ X-ray scattering spectra from PbTiO_3 films grown on single crystalline SrTiO_3 substrates reveal modulations only down to a 3 unit cell thick film, indicating that the limit for the existence of ferroelectricity in a PTO film is 3 unit cells in thickness.

Studies of Ferroelectric Phenomena in Perovskite Nanostructures

*O. Auciello, and D. J. Kim, Argonne National Laboratory
V. Nagarajan and R. Ramesh, University of Maryland*

Motivation—Theory indicates that an enhanced piezoelectric response should be observed if 90° ferroelastic domain walls move under electric field excitation in ferroelectric materials. Considering that removal of constraints due to film/substrate interaction may enable phenomena not hitherto observed in normal ferroelectric thin films that are laterally constrained by substrate-induced clamping, we have investigated polarization dynamic phenomena in LSCO/PZT/LSCO nanocapacitors fabricated with a focused ion beam (FIB) method down to 70×70 nm structures where film lateral constraints are removed. (LSCO= $\text{LaSr}_{0.5}\text{Co}_{0.5}\text{O}_9$). We also developed a top-down approach to produce ferroelectric nanocapacitors to study ferroelectric domain in capacitors produced by a method other than FIB to avoid beam damage.

Accomplishment—We investigated ferroelectric domain dynamics at the nanoscale, through evaluation of domain structure, stability, and relaxation as a function of ferroelectric layer microstructure and controlled capacitor size and geometry.

We used an AFM piezoresponse imaging method based on the detection of the local electromechanical vibration of polarized domains in a ferroelectric sample, caused by an external AC voltage applied between an atomic force microscope (AFM) tip (movable top electrode) and an electrode layer underneath the ferroelectric layer (Fig. 1a). The AC electric field with a frequency ω causes a localized sample vibration with the same frequency due to the piezoelectric effect.

The ferroelectric domain structure is visualized by monitoring the first harmonic signal (piezoresponse signal). Regions with opposite polarization orientation, vibrating in counter phase with respect to each other, under the applied AC field, appear as regions of different contrast in the piezoresponse image (Fig. 1c and d).

We found that nanostructuring of the ferroelectric layer can dramatically alter the electro-mechanical interactions between the film and the substrate thereby enabling the movement of the ferroelastic 90° domain walls. This movement can be facilitated by a break or large weakening in the film clamping to the substrate. Piezoresponse scanning force microscopy images clearly show that 90° domain walls can move. Furthermore, measurements of the d_{33} parameter for $\leq 1 \times 1 \mu\text{m}^2$ capacitors with such unclamped ferroelectric layers reveal values of up to 250pm/V at remanence, which is approximately 3-4 times the predicted value of 87pm/V for a single domain ferroelectric single crystal. We developed an e-beam lithography method to produce ferroelectric nanocapacitors (see figs 2 (a) and (b) and used the piezoresponse imaging technique to obtain ferroelectric polarization images on the nanocapacitors (see Fig. 2(c)).

Significance—From the fundamental science point of view, we demonstrated for the first time that 90° domains move in unconstrained ferroelectric thin films when sculpted into nanostructures. These results may have a major impact in the development of the next generation of high-density ferroelectric memories.

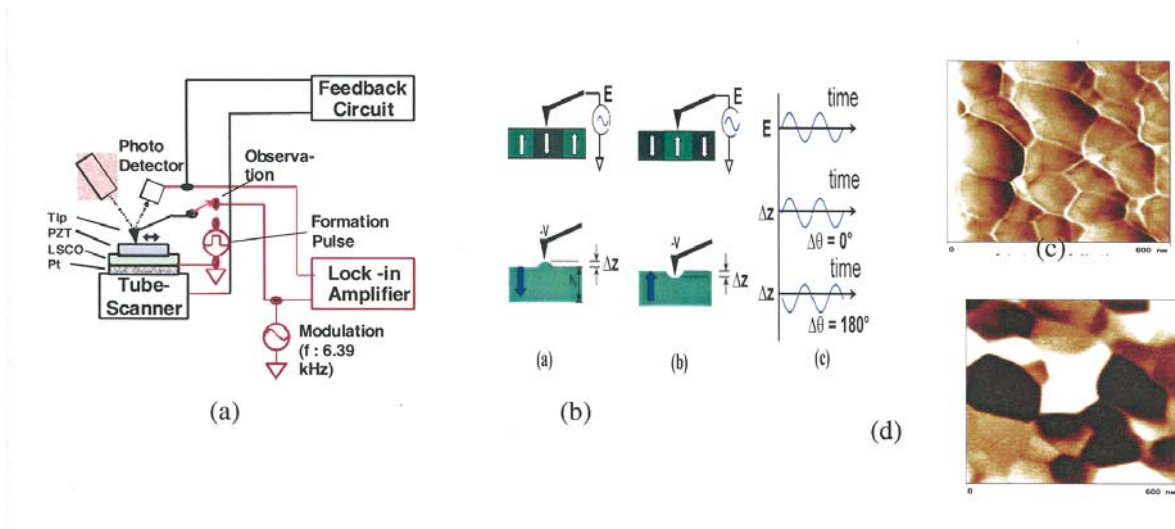


Figure 1. (a) Schematic of AFM piezoresponse imaging; (b) schematic of polarization domain created by DC electric field applied between AFM tip (top electrode) and bottom electrode layer, (c) topographical image; (d) piezoresponse image (white -polarization up and dark-polarization down).

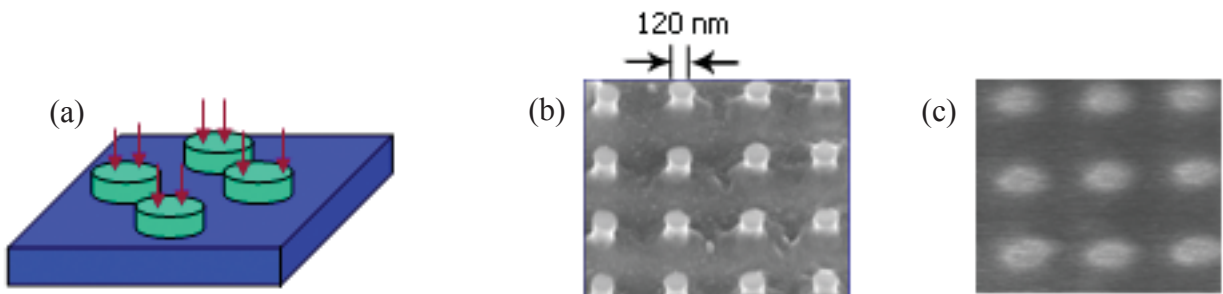


Figure 2. (a) Schematic of fabrication of nanocapacitors by e-beam lithography; (b) SEM picture of PZT nanocapacitors fabricated by FIB; (c) piezoresponse image showing polarization of nanocapacitors in (b).

High Energy Density/High Zirconia Content PLZT Films

B. A. Tuttle, G. Brennecka, D. Williams, T. Headley and M. Rodriguez,

Sandia National Laboratories, NM

Motivation—Miniaturization of electronic systems is an important driver for new dielectric materials with high dielectric constants, such as lead zirconate titanate (PZT). Thin films of these high dielectric constant materials offer the additional potential benefit of improved integration. Particularly intriguing possibilities can be realized in the future by combining next generation microelectromechanical systems (MEMS) with requirements for high energy density capacitors, with thin film dielectrics. Since present commercial capacitors are 10 to 100 times larger than most MEMS devices, the largest gain in miniaturization and performance is obtained by reducing the size and enhancing the integrability of the largest component in the system: the pulse discharge capacitors. High energy density capacitors based on high zirconia lead lanthanum zirconate titanate (HZPLZT) dielectric thin films are well suited for these potential applications. Critical materials issues are precise control of Pb stoichiometry and perovskite phase nucleation and growth at the nanoscale interface level, and the effect of these processing parameters on dielectric properties and breakdown behavior of the films.

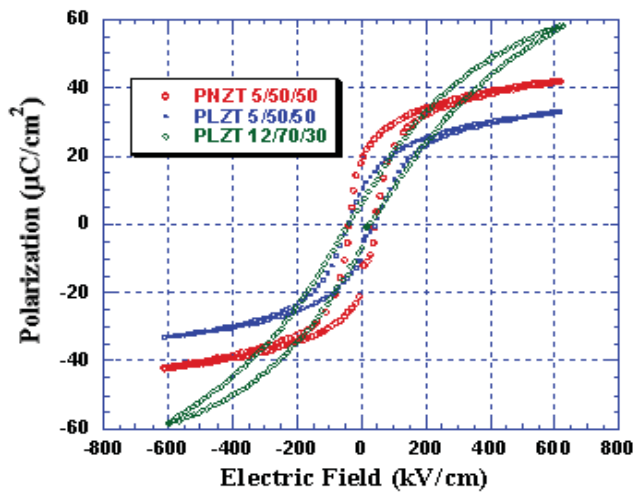
Accomplishment—As part of the Center for Synthesis and Processing, we have developed a reproducible process to fabricate high Zr content PLZT thin films, with compositions near the morphotropic phase boundary, that have twice the energy density of state of the art materials. These films possess dielectric constants in excess of 1100, breakdown fields of 1.5 MV/cm and energy densities of 16 J/cm³. Polarization versus electric field hysteresis behavior is shown in Fig. 1 for HZPLZT films versus state of the art near morphotropic phase boundary films. The HZPLZT films exhibit more linear behavior

at high fields, which enhances their energy density handling capability as shown in the table. The effect of the following process parameters have been studied: Pb stoichiometry, pyrolysis temperature, platinum vs. perovskite structure electrodes, seed layers, PbO atmosphere control, rapid thermal processing and PbO overcoat layers. Pyrolysis temperature was found to be the most critical parameter for obtaining high energy density films for this high PbO activity materials family.

Our processing studies indicated that a critical factor for reproducible film fabrication is accurate control of the Pb stoichiometry at the nanoscale level. Cross-sectional TEM micrographs in Fig. 2 show the differences of phase assemblages in films with dielectric constants (K) of 1100 versus films with K = 650. The lower dielectric constant film (Fig. 2a) has a fluorite second phase top layer. Conversely, the film with 40% higher dielectric constant (Fig. 2b) has no evidence of this low dielectric constant (K = 50) second phase. Measurements using thin film glancing angle X-ray diffraction were consistent with the TEM analyses. A critical finding is that formation of lead-rich fluorite phases leads to lower dielectric constant materials, similar to fluorite phases that are Pb deficient. Our studies indicate that precise control of Pb stoichiometry is essential for high energy density PLZT film fabrication.

Significance—High energy density dielectric thin films are an important class of materials with broad applicability to capacitor technologies that require miniaturization and integration. These materials can benefit technical areas from fuel cells to electric hybrid vehicles to military technologies.

Contact: Bruce A. Tuttle, Sandia National Laboratories, NM
Phone: (505) 845-8026, Fax: (505) 844-9781, E-mail: batuttl@sandia.gov



Film Description	Breakdown Strength (kV/cm)	Energy Density (J/cm ³)
PNZT 5/50/50	800	5
PLZT 5/50/50	1100	10
PLZT 12/70/30	1400	22

- Short Time Duration < 1 ms
250 µs linear ramp to breakdown
- All films 0.6 microns thick
- All electrodes 0.7 to 1 mm diameter

Figure 1. Polarization versus electric field behavior and energy density for SNL's HZPLZT thin films (PLZT 12/70/30) compared to state of the art near morphotropic phase boundary films.

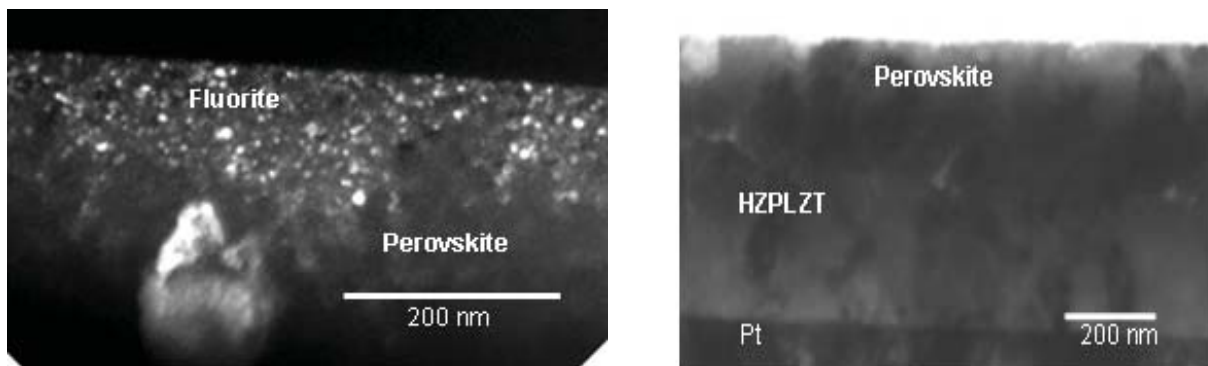


Figure 2. Cross-Sectional TEM Micrographs of (a) low dielectric constant HZPLZT film showing 80 nm thick, fine grain fluorite second phase at top film surface (dark field image) and (b) High dielectric constant HZPLZT films with no fluorite phase at top film surface (bright field image).

Nano-void Nucleation and Growth at the Aluminum/Oxide Interface as a Pre-pitting Process

K. R. Zavadil and P. G. Kotula, Sandia National Laboratories, NM
H. S. Issacs, Brookhaven National Laboratory

Motivation—The leading models for localized corrosion (pitting) invoke the presence and specific roles of nanoscale voids at the aluminum/oxide interface (1,2). To date, no direct observation of or measurements have been made on these nanostructures, and their presence has only been inferred based on the appearance of eventual micro- or mesoscopic features. Our goal in this work is to identify if nano-voids are a predominant structural feature in the passive oxide and to study whether they play a deterministic role in pit initiation.

Accomplishment—Our team is the first to experimentally validate that nanometer-sized voids do exist within the passive oxide on aluminum under pre-pitting electrochemical conditions (3). A combination of electrochemical, SEM and TEM techniques shows that these voids are one of several dominant nanostructural features that evolve in the oxide during electrochemical exposure prior to pit initiation. These voids nucleate at and grow from the Al/oxide interface, as shown in the transmission electron micrographs of Figure 1. Voids have an oblate hemispherical shape and do not appear to penetrate into the Al. We find that these voids are generalized to both single crystal Al and Al thin films (Fig. 2a) capped with both dry and solution-derived oxides. Void growth (areal density and size) correlate with the quantity of passive charge density generated with polarization, as shown in Fig. 2b.

We have completed kinetic studies looking at the impact of the thickness of the oxide prior to polarization, the rate of potential change and the extent of polarization in the absence of pitting to describe void growth. Our results show that pitting can take place across a broad range of void

size, including pores that transition from voids. Electrolyte comparison studies show that void formation is far more efficient in the presence of Cl⁻ compared to a variety of other common anions.

Our results show that nano-voids are a predominant structural feature in the passive oxide, but their characteristics do not match required elements of the leading pit initiation models. Constraint of the voids to the oxide eliminates the possibility that they represent the chloride-filled precursor sites that McCafferty proposes are necessary for pit initiation (2). The occurrence of vertical growth in these voids argues against a Point Defect Model-based view of initiation by 2-dimensional void formation, oxide detachment, and oxide thinning (1). The variability in void density and size observed with stable pitting shows that where these voids may be necessary for initiating pitting, their presence and eventual rupture are not alone sufficient to induce stable pitting.

Significance—We have defined a predominant nanostructural feature that may be the key constituent of the two leading models that attempt to describe pit initiation. Experiments can now be designed to test these models for validity and to provide knowledge to formulate new models or more accurately refine existing ones. The resulting enhanced understanding will allow the community to identify the extent to which the passive oxide is deterministic toward localized corrosion.

1. D.D. Macdonald, *Pure & Appl. Chem.* 71(6), 951 (1999).
2. E. McCafferty, *Corr. Sci.* 146, 1421 (2003).
3. K. R. Zavadil, et al. *J Electrochem. Soc.*, submitted.

Contact: Kevin R. Zavadil, Sandia National Laboratories, NM
Phone: (505) 845-8442, Fax: (505) 844-7910, E-mail: krzavad@sandia.gov

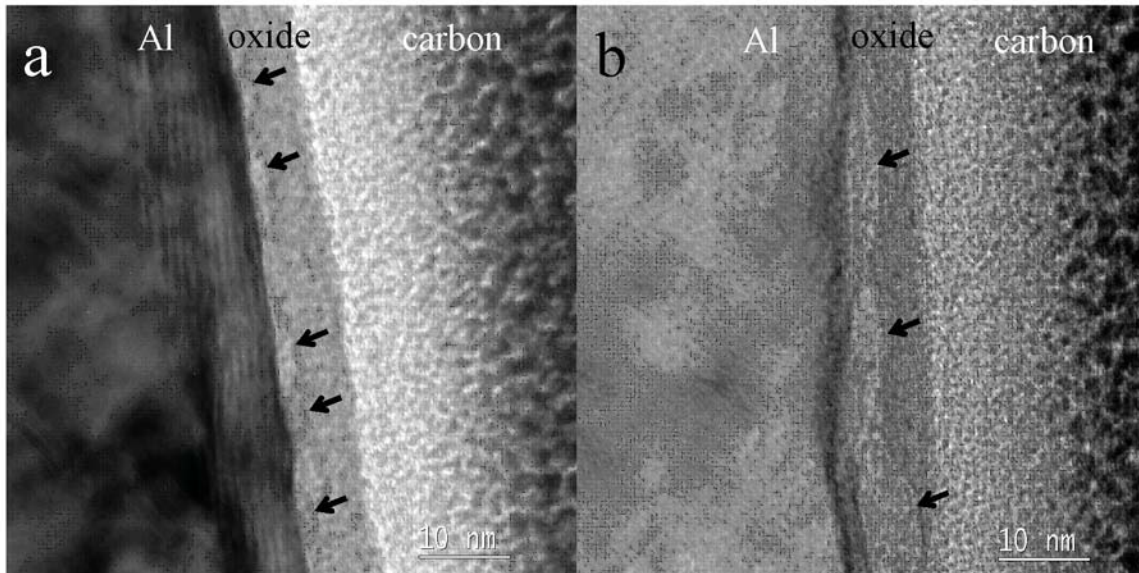


Figure 1. TEM images of sites on Al(110) exhibiting nano-void nucleation at the Al/Al₂O₃ interface - a) after an 13 hr open circuit hold followed by polarization to -495 mV producing 2.4 mC·cm⁻² and b) after a 4 hr open circuit hold followed by polarization to -518 mV producing 4.2 mC·cm⁻² of passive charge density. Arrows indicate location of voids. These voids are only observed under electrochemical conditions. Potentials are referenced to the SCE.

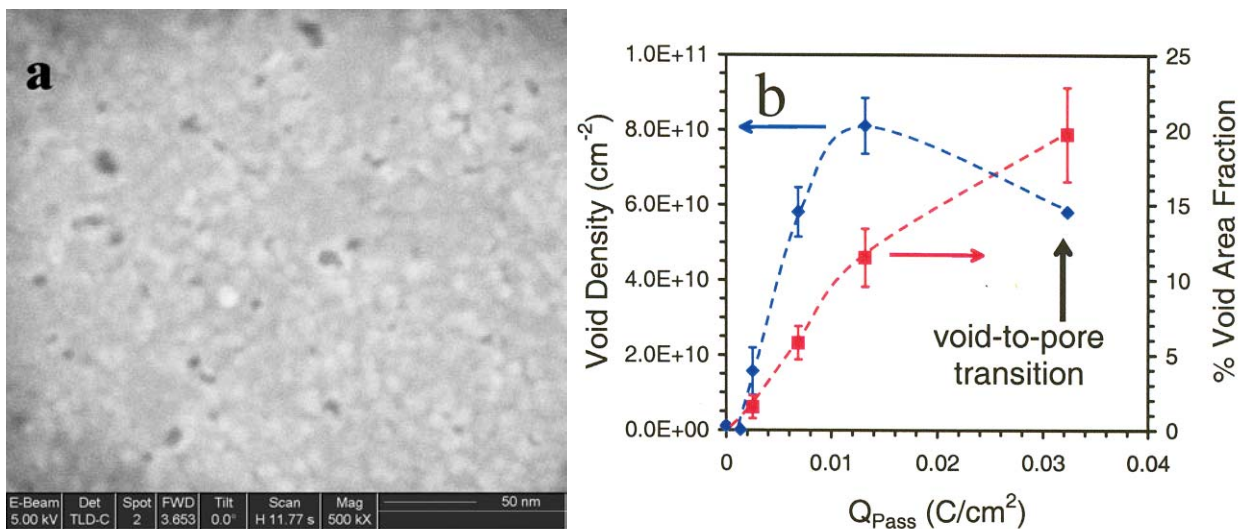
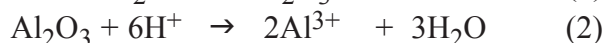
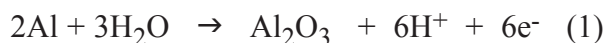


Figure 2. a) SEM images of a site on a nano-crystalline Al film after an 23 hr open circuit hold followed by polarization to -305 mV producing 2.5 mC·cm⁻² of passive charge density and b) the variation in void density (blue) and void area fraction (red) as a function of passive charge density generated during the polarization to pitting of a series of Al film sites. Dashed lines are a guide to the eye.

The Kinetics of Al₂O₃ Film Dissolution in Aqueous Chloride Solutions

Chett J. Boxley, Sungwon Lee, and Henry S. White,
University of Utah

Motivation—The thickness of the Al₂O₃ film on aluminum is governed by a dynamic balance of oxide growth (eq. (1)) and oxide dissolution (eq. (2)).



The presence of Cl⁻ in solution has been postulated to increase the rate of Al₂O₃ film dissolution, eventually leading to pit initiation. However, no quantitative measurements of the chemical kinetics of Al₂O₃ film dissolution in the presence of Cl⁻ have been reported. Quantitative measurement of the dissolution rate of the oxide film is necessary in predicting the stability of the Al/Al₂O₃ interface.

Accomplishment—Following the method of Isaacs and coworkers at Brookhaven National Laboratory,¹ we have developed voltammetric and amperometric methods to measure the chemical dissolution rate, R_{dis}, of thin (~3 nm) barrier-type Al₂O₃ films in neutral pH solutions containing Cl⁻. We have measured R_{dis} for high-purity polycrystalline^{2,3} and single-crystal electrodes⁴ (provided by Ames Laboratory) by fitting computer simulations of the electrochemical response to experimental data. In our computations, we assume high-field growth of the oxide film.² These experiments represent the first quantitative kinetic measurements of oxide film dissolution.

Figure 1 show an example of experimental and numerical voltammograms for an Al electrode in a borate solution (pH = 6.7). R_{dis} is obtained from the numerical fit; the excellent agreement between experiment and simulation validates the appropriateness of the model.

The dependence of R_{dis} on Cl⁻ concentration for polycrystalline Al is shown in Figure 2. For [Cl⁻

] < 5 mM, values of R_{dis} are indistinguishable from that measured in the absence Cl⁻, indicating that low-level concentrations of Cl⁻ have little effect on dissolution. R_{dis} increases and tends to a saturation value at high [Cl⁻], reminiscent of an adsorption-controlled process. A kinetic model that assumes a Langmuir adsorption isotherm and the involvement of two Cl⁻ anions in the rate limiting step of dissolution has been developed to interpret the dependence of R_{dis} on [Cl⁻].

R_{dis} has also been measured as a function of [Cl⁻] for the (111), (110), and (100) surface orientations of electropolished single-crystal Al electrodes. We find that R_{dis} is significantly higher at polycrystalline Al electrodes, suggesting that oxide disorder at grain boundaries significantly enhances the rate of dissolution.

Significance—The ability to quantify the kinetics of oxide dissolution by electrochemical methods provides a new means to address the relationship between the chemical stability of the oxide film and localized corrosion. We have recently measured both R_{dis} and the pitting potential of polycrystalline Al under identical solution conditions, and found that both quantities exhibit very similar dependencies on [Cl⁻].² Our results suggest pitting is inherently linked to R_{dis}. Our results are thus providing new clues in understanding the fundamental causes of localized corrosion.

1. H. Lee, F. Xu, C. S. Jeffcoate and H. S. Isaacs, *Electrochem. Solid-State Lett.*, **4**, B31 (2001).
2. C. J. Boxley, J. J. Watkins, and H. S. White, *Electrochem. Solid-State Lett.*, in press.
3. C. J. Boxley and H. S. White, *J. Electrochem. Soc.*, submitted.
4. S. Lee and H. S. White, *J. Electrochem. Soc.*, in preparation.

Contact: H. S. White, University of Utah

Phone: (801) 585-6256, Fax: (801) 581-5720, E-mail: white@chem.utah.edu

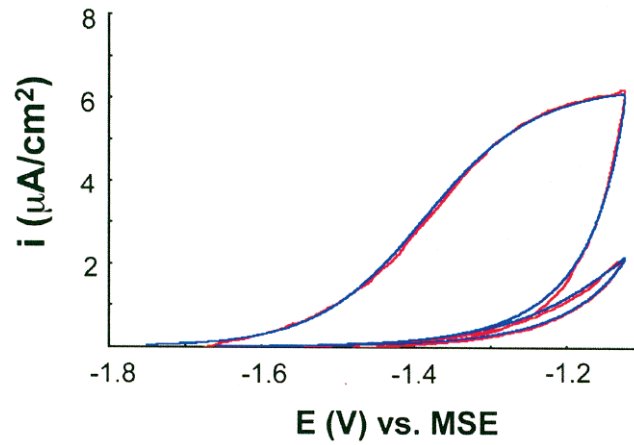


Figure 1. Experimental (red curve) and simulated (blue curve) voltammetric response of an Al electrode in a 50 mM H_3BO_3 / 0.3 mM $\text{Na}_2\text{B}_4\text{O}_7 \cdot 10 \text{H}_2\text{O}$ solution.

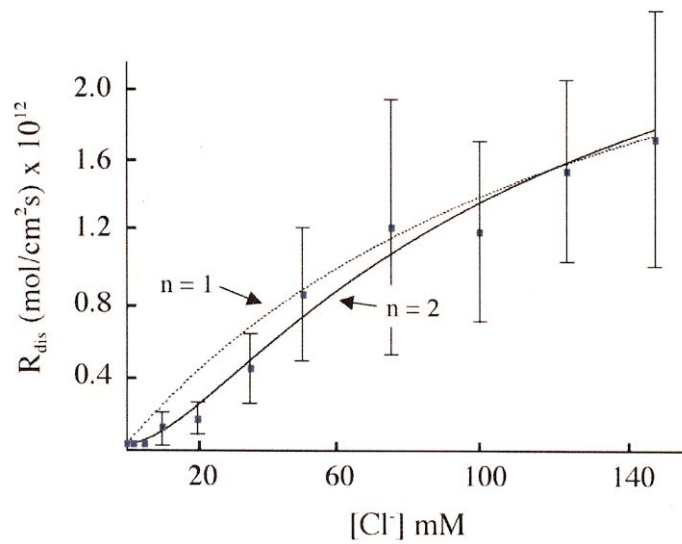


Figure 2. Rate of dissolution of the Al_2O_3 film (R_{dis}) as a function of Cl^- concentration. The lines labeled $n = 1$ and $n = 2$ correspond to trends expected for first and second order dissolution kinetics based on a competitive-adsorption Langmuir isotherm.

***Ab Initio* Modeling of Electrochemical Interfaces: The Double Layer and H₂O Reduction on Cu(111)**

*R. G. Kelly, C. D. Taylor, and M. Neurock,
University of Virginia*

Motivation—The physical scales of the important processes that control pitting corrosion range from the atomistic to millimeters. We are attempting to develop computational models at each of the appropriate size scales and then link them together to provide insights into the controlling processes as well as providing connections to other CSP experimental work. During the past year, we have focused on *ab initio* modeling of the structure of the electrochemical interface, following our work on continuum mass transport in 2001 and kinetic Monte Carlo modeling of pitting in 2002.

Accomplishment—We have calculated the atomistic structure of a $\sqrt{3}\times\sqrt{3}$ periodic three layer copper(111)-water interface over a range of cathodic and anodic potentials using density functional theory (DFT). The unit cell ($a=b=4.486\text{\AA}$, $c=19.75\text{\AA}$, $\alpha=\beta=90^\circ$, $\gamma=60^\circ$) is comprised of nine copper atoms, three in each layer, and eight molecules of water. Changes in dipole orientation and water activation were observed under the application of both double layer and cathodic conditions. These results represent the first successful *ab initio* modeling of a polarized, immersed interface on a corrodible metal. We used an approach to treating the polarized system that was recently pioneered at UVa [1].

The double layer region, bounded by oxide formation on the anodic side and hydrogen evolution on the cathodic side, is characterized by a weak copper-water surface interaction and by reorganization of the nuclei to accommodate the changing electronic charge. A flip-flop mecha-

nism for dipole reorientation (whereby a cathodic and anodic environments induce either H-facing or O-facing adsorption respectively) is here observed (Fig. 1) confluent with the results of Filhol and Neurock [1] and long standing electrochemical interpretation [2].

No chemisorptions are observed under cathodic conditions, in agreement with expectations of a bare Cu surface at potentials negative of its potential of zero charge. Little chemistry occurs until substantial cathodic polarization occurs. When 7 electrons are added to the unit cell, adsorbed hydride is observed, and when 9 electrons are added to the unit cell a second hydrogen molecule is evolved, apparently via a surface mediated reaction (Fig. 2).

Significance—These results open the door for an entire new thrust in electrochemical science by allowing the structural changes at a metal/solution interface to be mapped over a wide range of potential from first-principles calculations. Rationalization of speculations based on experimental measurements of interfacial processes has already been demonstrated. By linking these results with the kinetic Monte Carlo methods, the earliest stages of electrochemical reactions can be probed and their mechanistic pathways critically analyzed. Such information can then be used to design/select species to control the reactivity of the interface.

References

- [1] Neurock, M.; Filhol, J. S. *in preparation*.
- [2] Bockris, J. O.; et al. *Adv. Coll. & Interf. Sci.* 33, **1990**, 1-54.

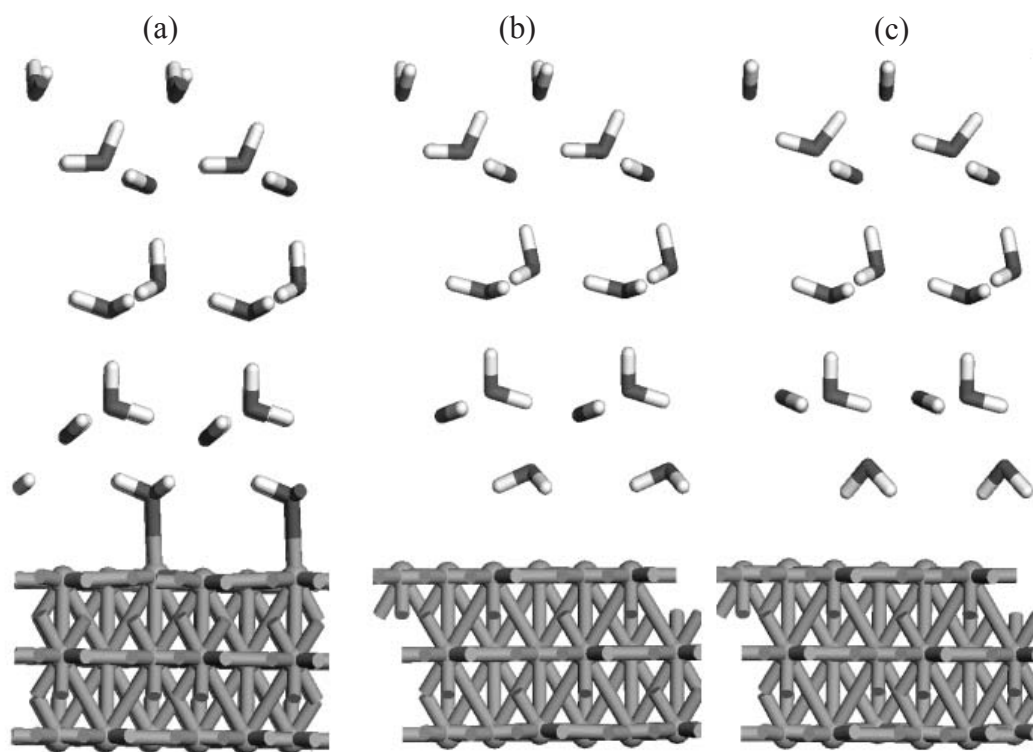


Figure 1. Reorientation of the interfacial water dipole from neutral (a) to cathodic potentials (b and c). Two electrons are added to a 9 Cu atom unit cell in **b** while three are added in **c**. H_2O molecules re-orient from an O down to a H down configuration with electron addition.

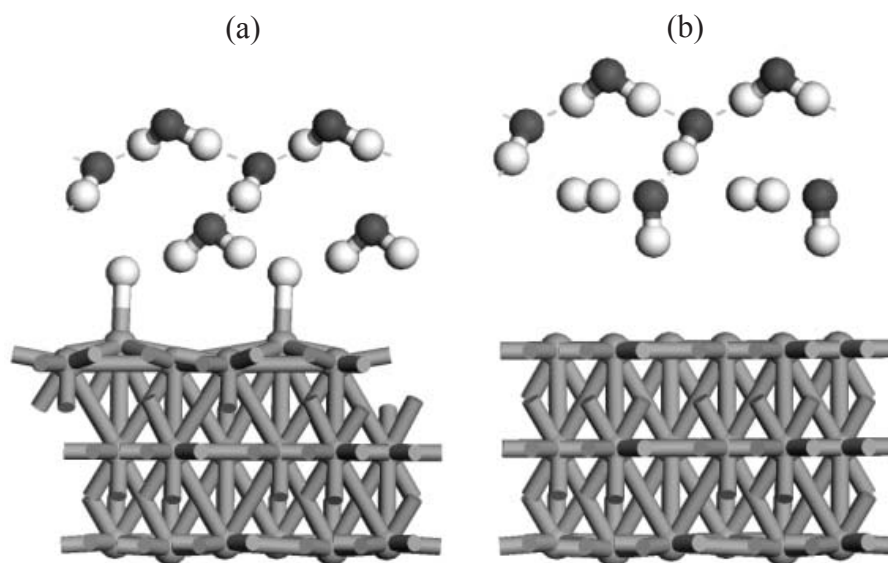


Figure 2. Formation of H_2 via a surface-hydride intermediate occurs between the addition of 8 (a) and 9 (b) electrons to the unit cell, left to right respectively. The surface hydride species is, however, first observed when 7 electrons were added to the unit cell.

Ab Initio Modeling of Electrochemical Interfaces: Underpotential Oxidation of Cu(111) in H₂O

R. G. Kelly, C. D. Taylor, and M. Neurock,
University of Virginia

Motivation—The physical scales of the important processes that control pitting corrosion range from the atomistic to millimeters. We are attempting to develop computational models at each of the appropriate size scales that can be linked together to provide insights into the controlling processes and connections to other CSP experimental work. In the past year, we have focused on *ab initio* modeling of the electrochemical interface, following work on continuum mass transport in 2001 and kinetic Monte Carlo modeling of pitting in 2002.

Accomplishment—We have calculated the atomistic structure of the copper(111)-water interface over a range of anodic potentials using density functional theory (DFT), in an approach recently pioneered at UVa [1]. Pathways were traced for the initial stages of oxide formation starting from the potential of zero charge. Changes in coordination mode, water activation and surface morphology were observed. Qualitative comparison to literature measurements was excellent, with bond lengths being quantitatively predicted. These results represent the first successful *ab initio* modeling of a polarized, immersed interface on a corrodible metal.

Deprotonation and migration of adsorbing water species upon Cu(111) smoothly transitions into oxidative chemistry at the interface under anodic polarization. As seen in Figure 1, the sequential removal of electrons from the model system prompts the following structural changes: A-top H₂O migrates to a bridging site followed by deprotonation to OH, which in turn migrates to hcp hollow. Further anodization results in a second deprotonation and shortening of the Cu-O bond (Figure 2, left). Under high levels of anodic polarization, extreme buckling of the surface

occurs and a copper atom is lifted out of the plane towards the adsorbed oxygen (Figure 2, center). Upon further charging oxygen displaces the ejected copper atom, effecting the formation of a stoichiometric Cu₂O monolayer with a closely bound Cu-H₂O complex (Figure 2, right). These changes represent the early signs of corrosion in acidic media.

These findings correspond well with a wide variety of current observations of the Cu-H₂O interface, including SERS measurements of the deprotonation of adsorbed OH on Cu to form what was conjectured to be a subsurface oxide [2] the presence of two types of adsorbed OH [3], the ejection of mobile Cu adatoms synchronous with adsorption of oxide [4], specular X-ray reflectance measurements of Cu-O bond distances [5]. The ability to reconcile this considerable range of data *via* computation speaks well of the versatility offered by DFT.

Significance—These results demonstrate the viability of *ab initio* methods to map the structural changes at a metal/solution interface over a wide range of potentials. Further calculation of energetic barriers can then be used in conjunction with continuum and KMC models to design/select species to control the reactivity of the interface.

References

- [1] Neurock, M., and Filhol, J. S. *In preparation.*
- [2] Hartinger, S., *et al.* *J. Electroanal. Chem.* **397**, 1995, 335-338
- [3] Niaura, G. *Elect. Acta.* **45**, 2000, 3507-3519
- [4] Chan, H. Y. H., *et al.* *J. Phys. Chem. B.* **103**, 1999, 357-365
- [5] Robinson, I. K. *Unpublished Data.*

Contact: Robert G. Kelly, University of Virginia
Phone: (804) 982-5783, Fax: (804) 982-5799, E-mail: rgkelly@virginia.edu

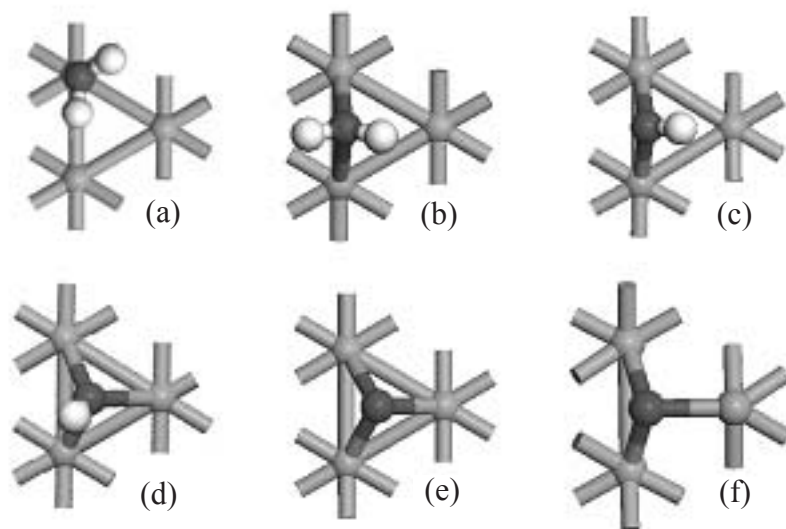


Figure 1. Top views of adsorbed species illustrating the progressive migration and deprotonation of water at the surface under increasingly anodic conditions as electrons are successively removed: (a)-(e) 0-4 electrons removed respectively, (f) 7 electrons removed.

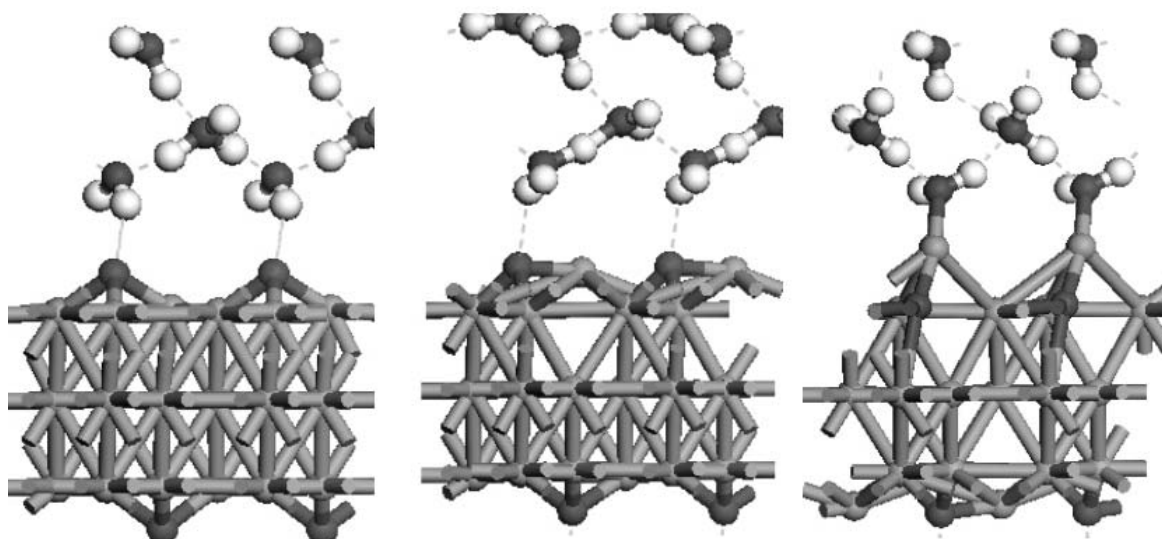


Figure 2. Oxide adsorption at 4 electrons removed (left), surface reconstruction at 7 electrons removed (center), and early Cu dissolution surface complex (right, 10 electrons removed).

Intrinsic and Materials Effects on the Thickness Dependence of J_c in YBCO Coated Conductors

R. Feenstra, A. A. Gapud, D. K. Christen, E. D. Specht, and A. Goyal,
Oak Ridge National Laboratory

T. G. Holesinger, and P. N. Arendt, Los Alamos National Laboratory

D. M. Feldmann, A. Gurevich and D. C. Larbalestier, University of Wisconsin

Motivation—Coated conductors (CCs) are being developed as a technology for fabricating wires of the moderately anisotropic, $T_c=90$ K superconductor $\text{YBa}_2\text{Cu}_3\text{O}_7$ (YBCO). These conductors are capable of strongly-linked current flow at substantial levels compared to intrinsic limits. In this technology, the YBCO is provided in the form of an epitaxial film, which is deposited onto a suitably configured, biaxially textured substrate tape through continuous processes. To successfully make the transition from a thin-film technology to wires, the YBCO coating needs to have a significant thickness $d > 1 \mu\text{m}$ to provide the large currents needed for power applications. It is observed, however, that the critical current density J_c decreases with the YBCO layer thickness, reducing the efficiency by which I_c , the critical current, is increased. Both materials effects and effects due to the physics of flux pinning in quasi-two-dimensional systems ("intrinsic") are expected to play a role, but it is unknown to what extent.

Accomplishment—In large part the uncertainty regarding the origin of the thickness dependence of J_c is due to the unresolved nature of the flux pinning mechanism in these YBCO coatings. It is anticipated that different defect geometries may lead to different functional dependences of J_c on d . On the other hand, both the defect structure giving rise to flux pinning and defects (flaws) obstructing current flow are processing dependent. A simplifying assumption in flux pinning models is that the latter defects are essentially absent. Furthermore, a thickness independent defect density is assumed, with homogeneous distribution through the layer thickness. We have generated

a dataset for YBCO CCs that shows a strong J_c - d dependence for films produced to variable thickness. This dependence (Fig. 1) is satisfactorily described by a function $J_c \propto 1/d^{1/2}$. This latter dependence has been predicted from a collective pinning model of randomly distributed point defects. However, upon thinning of a thick-film specimen by ion milling and measuring J_c at each new thickness, a significantly weaker J_c - d dependence was found (Fig. 2). The fact that these two dependences do not agree violates model assumptions, and calls into question applicability of the collective pinning model. Microstructural analysis by TEM reveals that this film contains a bimodal growth structure with large grains (apparently grown from a liquid) in the bottom part of the film, and smaller, defective grains in the top (Fig. 3). Similar structures were observed in other, similarly processed, thick YBCO coatings. The results suggest that the thickness dependence of J_c for these films is primarily a materials effect associated with the liquid-mediated growth.

Significance—Upon reexamination, several published J_c - d datasets for YBCO films grown by alternative deposition techniques were found to agree with a $J_c \propto 1/d^{1/2}$ functional dependence. On the other hand, weaker J_c - d dependences also have been reported. This work and this collaboration provide a framework for analysis of the underlying differences. The study shows that, in addition to further experimental work, there is a need for theoretical modeling of thickness dependent effects in the flux pinning, taking into account variable defect structures, densities, and distributions.

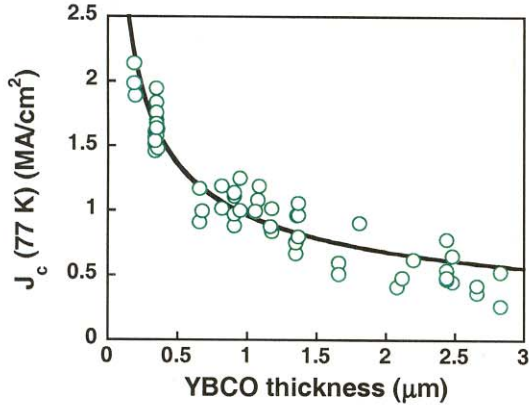


Figure 1. Thickness dependence of the critical current density J_c in $\text{YBa}_2\text{Cu}_3\text{O}_7$ (YBCO) epitaxial films deposited onto rolling assisted biaxially textured substrates (RABiTS). The substrates consisted of thermo-mechanically textured Ni-3at%W tape, coated with epitaxial layers of Ni, Y_2O_3 , YSZ, and CeO_2 . The YBCO coatings were grown by an *ex situ* BaF_2 process, using precursor layers deposited by three-source electron-beam evaporation. The precursors were furnace annealed to form the epitaxial YBCO structure. The line represents a fit to the data according to $J_c = 1.63 (0.35/d)^{1/2}$. In this expression, the factor 1.63 MA/cm^2 corresponds to the average J_c value measured for $0.35 \mu\text{m}$ thick films at 77 K in nominal self-field.

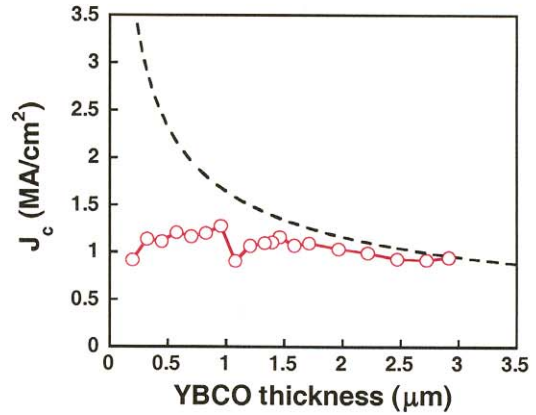


Figure 2. Through-thickness variation of J_c in a $2.9 \mu\text{m}$ thick *ex situ* YBCO coating on IBAD-YSZ coated conductor template. The biaxially textured yttria-stabilized zirconia (YSZ) layer of the template was produced by ion-beam assisted deposition (IBAD). J_c was measured at various thickness values, obtained after thinning of the specimen by ion milling. The dashed curve represents a function $J_c \propto 1/d^{1/2}$ describing the dependence observed for variable thickness films (similar to Fig. 1). It is evident that the through-thickness J_c exhibits a weaker dependence on d . The bottom layer of this thick film apparently has a lower J_c than a similarly thick film produced from thin precursor.

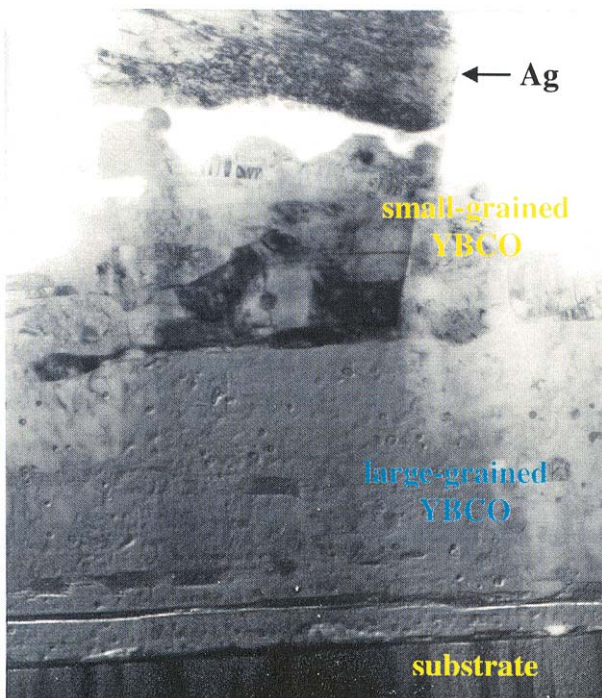


Figure 3. Cross section transmission electron micrograph (TEM) of a $2.9 \mu\text{m}$ thick *ex situ* YBCO coating on IBAD-YSZ, similar to the sample of Fig. 2. The image shows a bimodal structure in the YBCO, consisting of single-crystal-like, large grains near the substrate interface, and smaller, defect-rich grains near the surface. Similar bimodal structures were observed for films on RABiTS having $d > 2 \mu\text{m}$. Based on further details of this and other images, including chemistry of identified secondary phases, it is concluded that the different structures result from a bimodal growth mode, induced by a variable role of Ba-rich liquids in the precursor conversion process.

AC Losses in Circular Disks of $\text{YBa}_2\text{Cu}_3\text{O}_7$ Films in Perpendicular Magnetic Fields

*M. Suenaga, and Q. Li, Brookhaven National Laboratory
S. R. Foltyn, and H. Wang, Los Alamos National Laboratory
J. R. Clem, Ames Laboratory*

Motivation—With the impressive development of so-called "coated conductors" using a high-critical-temperature superconductor, $\text{YBa}_2\text{Cu}_3\text{O}_7$ (YBCO), a number of applications such as power transmission cables, transformers, and generators are being planned using these conductors. In these devices, ac losses in the superconductors will play a very important role in determining their efficiencies and, thus, their technological viability. Furthermore, the perpendicular component of the ac magnetic fields in these devices dominates the losses in most cases, since these YBCO conductors are made in the form of thin tapes with large aspect ratios. As illustrated in Figure 1, the magnetic field penetration is significantly different in a thin disk as contrasted with long cylinders which were studied extensively in the past. This difference is manifested in a very different magnetic field dependence of the losses in a film from that for a cylinder. Thus, it is important to understand the behavior of YBCO films in perpendicular ac magnetic fields. Previously, we reported measurements of ac losses in 1- μm thin-film YBCO circular disks in perpendicular ac applied magnetic fields.¹ We found that the losses agreed very well with the theoretically calculated losses using the field-dependent critical-current model.² Since the theory predicts a strong dependence of the losses on the thickness of the films at low fields, it is important to make a further test of the theory by investigating the thickness dependence of the losses.

Accomplishment—The ac losses in three disk-shaped $\text{YBa}_2\text{Cu}_3\text{O}_7$ films were measured in perpendicular applied ac magnetic fields to ~ 0.14 T at 10 Hz in liquid nitrogen. These films were deposited on SrTiO_3 by a pulsed-laser-deposi-

tion technique and had thicknesses d of 0.2, 1.0, and 3.0 μm .³ The losses at low fields were found to be a strong function of the film thickness as shown in Figure 2. The measured losses were compared with the theoretically calculated losses. The ac losses calculated using a field-independent (Bean model) critical-current density² agreed very well with the experimental values for the 0.2 μm -thick film, while the calculated losses agreed well when a field-dependent critical-current density, the Kim model, was used for the films of thickness 1.0 and 3.0 μm . The Kim-model critical-current density is defined as $J_{cK}(B_a) = J_c(0)/(1 + B_a/B_0)$, and $J_c(0)$ is the critical-current density at applied magnetic field $B_a = 0$. The comparisons of the theoretically calculated and experimental ac losses are given in Figure 3 (a) and (b) for 0.2 and 1.0 μm thick films, respectively.

Significance—This work⁵ and Ref. 1 together completed a thorough test of the theories on ac losses of thin superconducting films in perpendicular magnetic fields. These studies showed for the first time that these theories are applicable to the determination of the losses from YBCO films in perpendicular magnetic fields. This will make a strong basis for understanding ac losses in electric devices using YBCO coated conductors.

1. M. Suenaga, et al. *J. Appl. Phys.* **94**, 502 (2003).
2. D. V. Shantsev, et al *Phys. Rev. B* **61**, 9699 (2000).
3. S. R. Foltyn, et al. *Appl. Phys. Lett.* **75**, 3692 (1993); *Appl. Phys. Lett.* **82**, 4519 (2003).
4. J. R. Clem and A. Sanchez, *Phys. Rev. B* **55**, 9355 (1994).
5. M. Suenaga, et al. *J. Appl. Phys.* Accepted for a publication.

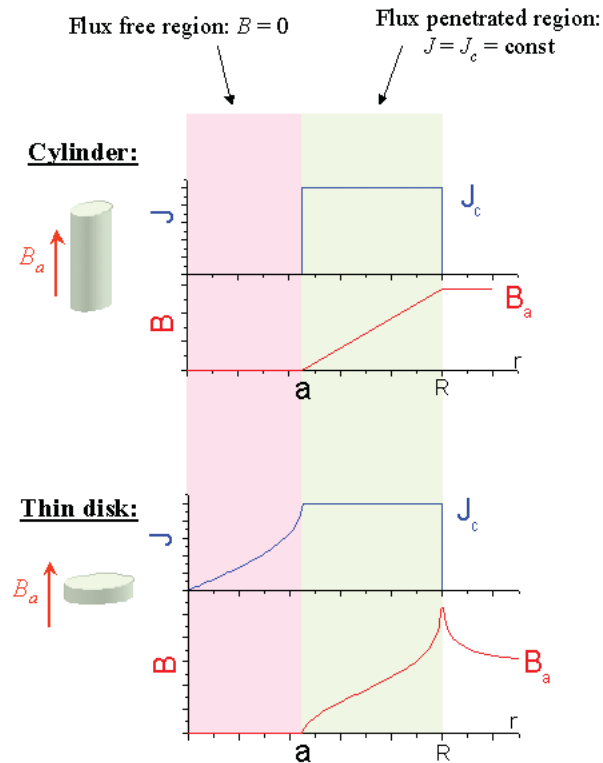


Figure 1. Magnetic fields B_a and current J_c profiles in a cylinder and a thin circular superconductor.

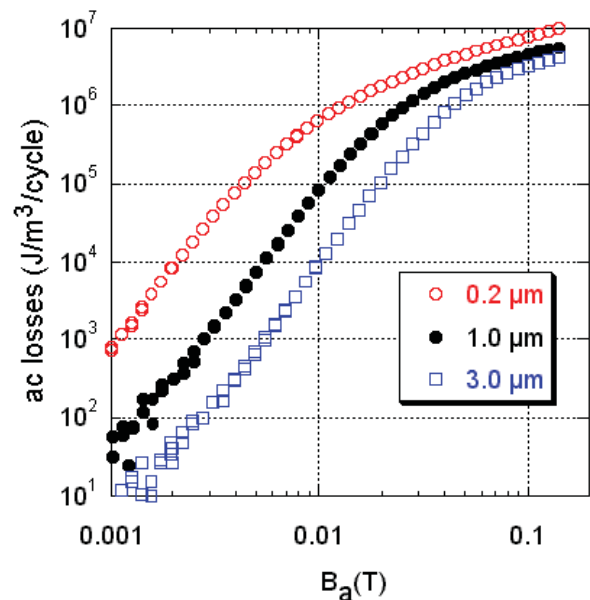


Figure 2. AC losses measured at 10 Hz and 77 K in perpendicular ac magnetic fields as a function of applied ac field amplitude B_a for YBCO films having thicknesses of 0.2, 1.0, and 3.0 μm . This shows that the losses are a very strong function of film thickness at low fields as predicted by theories.

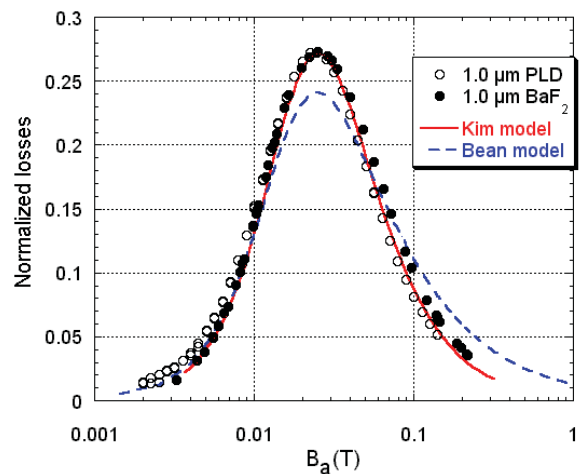
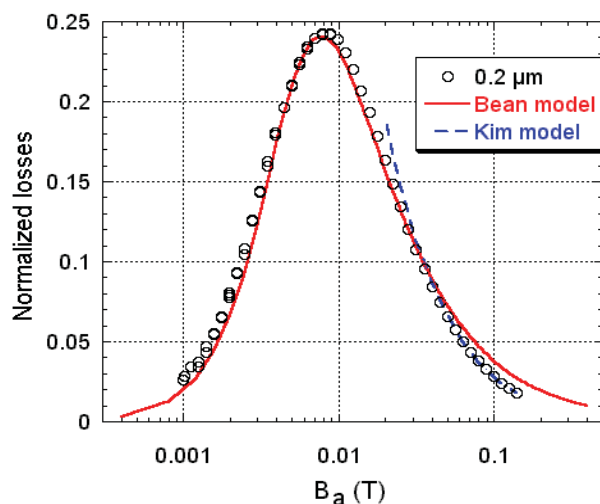


Figure 3. (a) Measured normalized losses for a 0.2 μm -thick film as a function of applied field B_a compared with numerically calculated losses using the Bean-model critical-current density and the fitted high-field approximation for the Kim-model critical-current density. (b) Normalized losses for 1.0 μm -thick films prepared by PLD and BaF_2 processes compared with calculated losses using the Bean and Kim models.

Reel-to-Reel Characterization of Time-Based Phase Evolution in YBCO Coated Conductors: The BaF₂ Precursor

*D. F. Lee, K. J. Leonard, L. Heatherly, S. Cook, and M. Paranthaman,
Oak Ridge National Laboratory*

V. A. Maroni, K. Venkataraman, and M. Mika, Argonne National Laboratory

Motivation—Results on YBCO coated conductor (CC) in excess of one meter lengths with high I_c 's are slowly emerging. In the ex-situ approach, the fabrication of multi-meter lengths of CC is generally being accomplished by deposition of a suitable YBCO precursor mix onto buffered/textured metal tape, followed by heat treatment of the coated tape to produce a biaxially textured film of orthorhombic YBCO. However, there is still no broadly recognized understanding of the mechanism involved in the YBCO precursor conversion, and, concomitantly, there is a need for an on-line diagnostic that can provide critical information about the progress and the quality of the CC fabrication process. The aims of this work are to identify potential feedback-control techniques, and to investigate phase evolution during the reactive heat treatment of meter-length tapes coated with the "BaF₂"-type precursor to the YBCO phase.

Accomplishment—Our approach is to combine the expertise in long-length "BaF₂" precursor deposition and reel-to-reel (R2R) x-ray diffraction (XRD) at ORNL with the R2R Raman microscopy capability at ANL. To facilitate sample fabrication, we have developed and tested a method for creating a graded Y-Ba-Cu-O phase assemblage on a single "BaF₂" precursor tape. This methodology involved slowly reeling a coated tape into a preheated furnace, such that the time at the prescribed treatment temperature varied in a systematic way along the length of the tape, then rapidly backing the tape out of the furnace to quench in the various states of YBCO phase evolution. The time domain expressed in these "quenched tape" experiments ranged from the very early stages of precursor crystallization to stages that involved (1) the initial formation

of YBCO, (2) the time domain of optimally converted YBCO, and (3) time domains past the optimum. These samples have subsequently been analyzed by R2R XRD (Fig. 1) and R2R Raman microscopy (Fig. 2). Figure 3 shows the R2R XRD of BaF₂ reactant and YBCO product from a 0.3 μ m precursor tape. It can be seen from this figure that the optimum processing time based on YBCO intensity is \sim 80 min. While XRD can provide texture and information on major phases, it is not suited for detection of intermediate products (as identified by TEM). On the other hand, while Raman microscopy is not ideal for texture determination, it can readily identify various transitional phases. Figure 4 shows the Raman measurement performed on the same tape. It can be seen from this figure that various phases such as BaF₂, Y₂Cu₂O₅, CuO etc. can be identified and tracked as the precursor reaction proceeds. Figure 5 shows the later stage of conversion where Raman identified the optimal processing time as 70-85 min. To validate these results, 1 cm sectional I_c measurement on a similarly processed tape (Fig. 6) was performed, which confirmed that J_c is fully developed in \sim 78 min. Similar tests were performed on a 1 μ m thick precursor tape, with the XRD, Raman, I_c -derived optimum times of 220 min, 185-220 min, and 210 min, respectively.

Significance—Process monitoring and control strategies of the DOE Coated Conductor Development Roadmap have stressed the importance to develop in-line in situ control techniques for large scale manufacturing. We have identified two potential candidates and the information that they can provide. Further development and testing of in-situ systems will satisfy this important goal.



Figure 1. R2R XRD system being developed at ORNL.

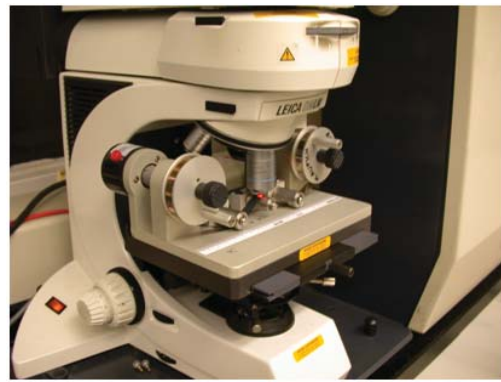


Figure 2. R2R Raman microscopy prototype developed at ANL.

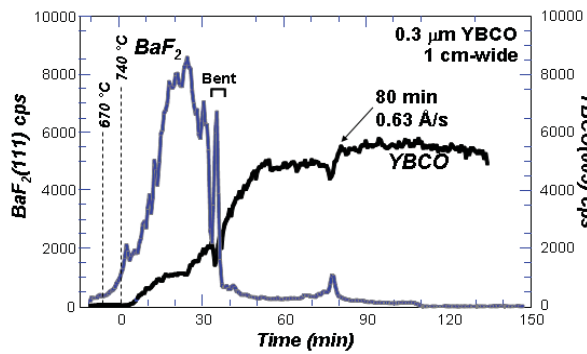


Figure 3. R2R XRD intensities of BaF_2 and YBCO as functions of conversion time.

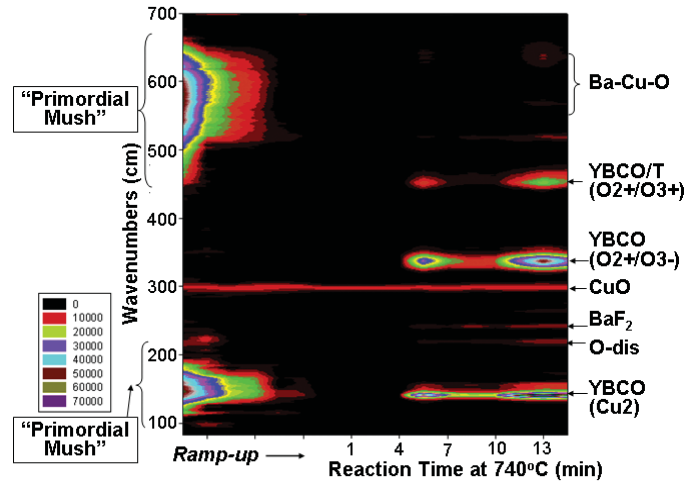


Figure 4. R2R Raman intensities of the same 0.3 mm precursor tape during the initial stage of YBCO formation.

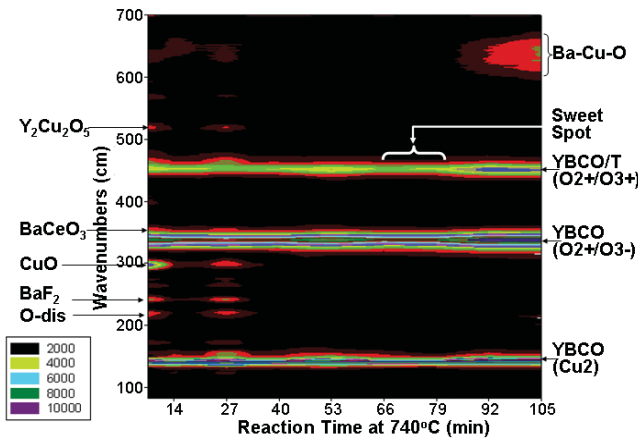


Figure 5. R2R Raman intensities of the 0.3 mm precursor tape during later stage of YBCO formation.

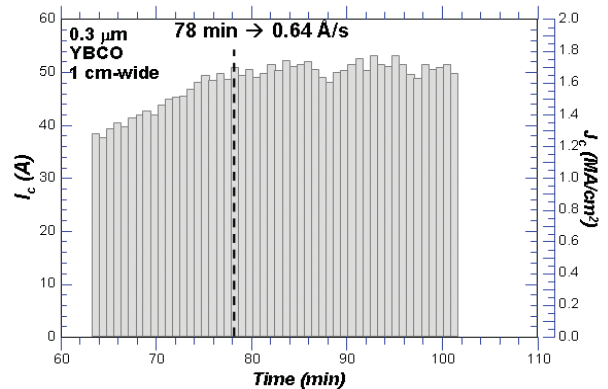


Figure 6. 1-cm sectional I_c 's of a 0.3 mm precursor converted under similar processing conditions.

Low-Temperature Growth of Ultrananocrystalline Diamond Thin Films

X. Xiao, J. Birrell, J. E. Gerbi, O. Auciello, and J. A. Carlisle, Argonne National Laboratory
R. J. Nemanich, North Carolina State University

Motivation—Materials integration is the key issue for any thin film material if it is to be used in applications, and has been a major impediment for diamond films in particular. This is mainly due to the relatively high growth temperatures (T) needed to grow good quality diamond films (typically 800°C). Over the past several years a new plasma/growth chemistry has been developed at ANL using *argon-rich* Ar/CH₄ plasmas. The C₂-dimer chemistry involved in this process, that leads to the growth of ultrananocrystalline diamond (UNCD) films, has a very low activation energy (< 5 kcal/mole), which has enabled the growth of diamond films at 400°C. The focus of this CSP work is to examine the nanoscale structure of these low-T UNCD films, and to develop seeding procedures that lead to very high initial nucleation densities, which are necessary in order to grow continuous, pinhole-free films at low temperatures.

Accomplishment—Low T (400°C) deposition of UNCD films with relatively high deposition rate (0.2 μm per hour) and low intrinsic stress has been achieved by using microwave plasma chemical vapor deposition (MPCVD). Conventional processes for the preparation of diamond films involve a high flow rate of hydrogen, such as HFCVD and MW-PECVD, require an elevated deposition T higher than 700°C, which notoriously limits the application of UNCD in electronic and MEMS devices. We have used our patented UNCD process with Ar/CH₄ as precursors, which greatly reduced the extra heating effect resulting from the hydrogen plasma. The optimized seeding process (ultrasonic vibration in the suspension of nano-diamond powders) increased the initial nucleation density (up to 1 × 10¹¹/cm²), thus greatly decreasing the time needed for the coalescence

of grains to form dense continuous films. This seeding process also has the advantage of being applicable to devices with complex contours and not producing any surface damage. Various characterization methods (UV, visible Raman, HRTEM, EELS, NEXAFS, XRD) confirmed that the films grown at 400°C consisted of 5~10 nm, phase pure diamond grains and 0.5 nm wide grain boundaries (Figs. 1 & 2), compared to the microstructure of the high T UNCD films (grain size: 2~5 nm, atomically abrupt grain boundaries). Synchrotron Radiation near-edge x-ray absorption fine structure (NEXAFS) measurements (Fig. 2) showed that the sp³ to sp² bonding ratio actually increased slightly as the growth T was lowered. Systematic studies on the influence of deposition T showed that the hydrogen desorption from the depositing surface played an important role in the nanostructure development of UNCD coatings. The currently observed high growth rate of 0.2 μm/hr (Fig. 3) is mainly attributed to the nano-diamond powder seeding process, which enhances the initial nucleation density and leads to further enhancement of the secondary nucleation.

Significance—These low-T UNCD films are expected to possess excellent mechanical, chemical and tribological properties equivalent to those of the typical high T UNCD. This result allows stress-free films to be deposited at Ts low enough to be compatible with the Si-based circuit components, which may enable diamond MEMS on CMOS chips, and also as an anti-stiction coating (stiction is the resistance to the start of motion). These films are also currently being developed for use as a bio-inert hermetic coating for a retinal prosthesis in a project funded by DOE-OBBER (Fig. 3).

Contact: J. A. Carlisle, Argonne National Laboratory
Phone: (630) 252-3520, Fax: (630) 252-9555, E-mail: Carlisle@anl.gov

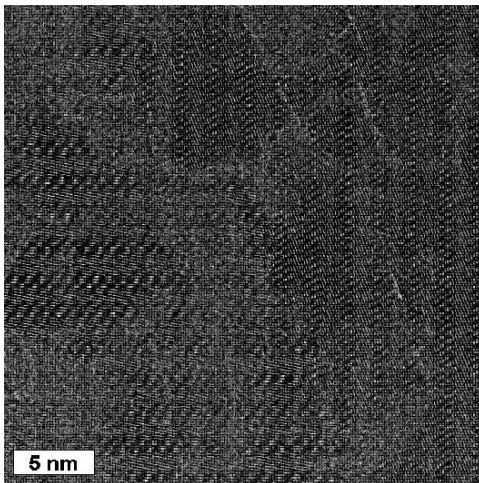


Figure 1. HRTEM image of a UNCD film grown at $\sim 400^\circ\text{C}$. The grain sizes observed are between 4-12 nm (8 nm average) and the grain boundary widths are about 0.5 nm, which are both very similar to films grown at 800°C .

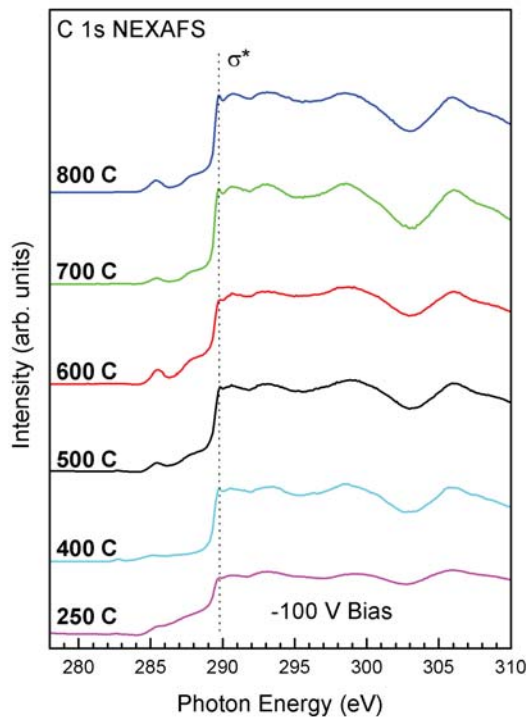


Figure 2. Near-edge x-ray absorption fine structure (NEXAFS) data obtained from a series of UNCD films grown at different temperatures. These data show the density of unoccupied electronic states, and a perfect diamond reference sample would have no features near 286 eV and a sharp core exciton near 290 eV. With its 3-5 nm grains and abrupt grain boundaries, UNCD normally consists of about 5% sp^2 bonding. These data indicate that in fact as the growth temperature is lower the sp^3/sp^2 bonding ratio actually increases.

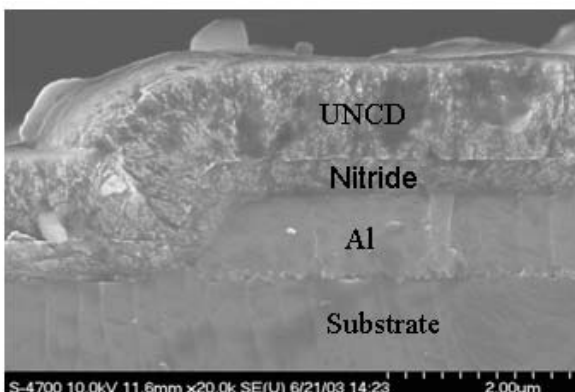


Figure 3. A UNCD film grown at $\sim 400^\circ\text{C}$ onto a patterned thin film heterostructure consisting of Al lines encapsulated by a SiN thin film on a silicon substrate. The growth time was 3 hours, with a resulting growth rate of $\sim 0.6 \mu\text{m/hr}$. Note the film is fully dense and highly conformal. No hillocks were observed in the Al lines.

Nanotribology and Surface Chemistry of Carbon-Based Films

R. W. Carpick, A. V. Sumant, and D. S Grierson, University of Wisconsin-Madison
J. A. Carlisle and O. Auciello, Argonne National Laboratory

Motivation—The chemical and tribological properties of carbon-based materials display a range of important mechanical, tribological and electronic characteristics. Films such as ultrananocrystalline diamond (UNCD) and diamond-like carbon can be fabricated to exhibit properties including unrivaled stiffness and hardness, low friction, high thermal conductivity, hydrophobicity, atomic-scale smoothness, and biocompatibility. Due to these properties, which far exceed those of silicon, possible applications include high performance materials for micromachines, field-emission devices, biocompatible sensors and actuators, and nano-engineered coatings with high hardness and low friction for a range of industrial applications.

We believe that surface chemistry and tribological properties are intimately linked. Our goal is to conduct AFM and surface spectroscopic measurements to determine the nature of this relationship, specifically for UNCD and diamond-like carbon films.

Accomplishment—We have shown that the exposed underside of UNCD films has a unique morphology that reflects its nucleation and growth characteristics. Clusters (100-400 nm in diameter) of grains (each <10 nm) grow and coalesce, pinching off narrow "crevice"-like voids which involve more sp²-bonded carbon than UNCD intrinsically has. The clusters, or "supergrains", are separated by crevices <50 nm in width and up to at least 80 nm deep. Within a supergrain, the roughness is extremely low, ~1 nm RMS. AES and PEEM/ NEXAFS (spatially resolved) spectroscopy reveal the enhanced sp²

character of the underside. XPS shows substantial oxygen as well. This oxygenated, graphitic layer will likely be tribologically problematic. So, we pursue strategies to restore a more purely "diamond" character to the underside. A hydrogen plasma treatment greatly reduces the oxygen, removes most of the sp²-bonded carbon, and leaves the surface H-terminated. Correspondingly, the nano-scale adhesion energy between WC AFM tips and UNCD drops by a factor of 2, from approximately 55 to 32 J/m², as measured in air. This is in the realm of van der Waals energies, indicating that we have reduced adhesion to near its lowest limit. Interestingly and quite tantalizingly, comparisons with single-crystal diamond surfaces indicate that UNCD *may have lower adhesion than pure diamond*. We hypothesize that the nano-scale roughness of the UNCD films may reduce the contact area between the tip and sample, thus reducing adhesion. Friction studies are currently underway, with preliminary results indicating that friction is also reduced due to H-termination.

Significance—The results indicate that controlling the surface chemistry of UNCD can result in large changes in nano-scale adhesion and probably friction as well. This points the way toward strategies for optimizing the material for MEMS and NEMS applications. It also shows that a basic science approach, combining surface spectroscopy, AFM microscopy and nanotribology, and processing schemes, can lead to meaningful design rules for micro- and nanodevices made of these advanced materials. It also provides support for schemes aimed at designing UNCD AFM cantilever probes.

Contact: R. W. Carpick, University of Wisconsin-Madison
Phone: (608)-263-4891, Fax: (608)-263-7451, E-mail: carpick@engr.wisc.edu

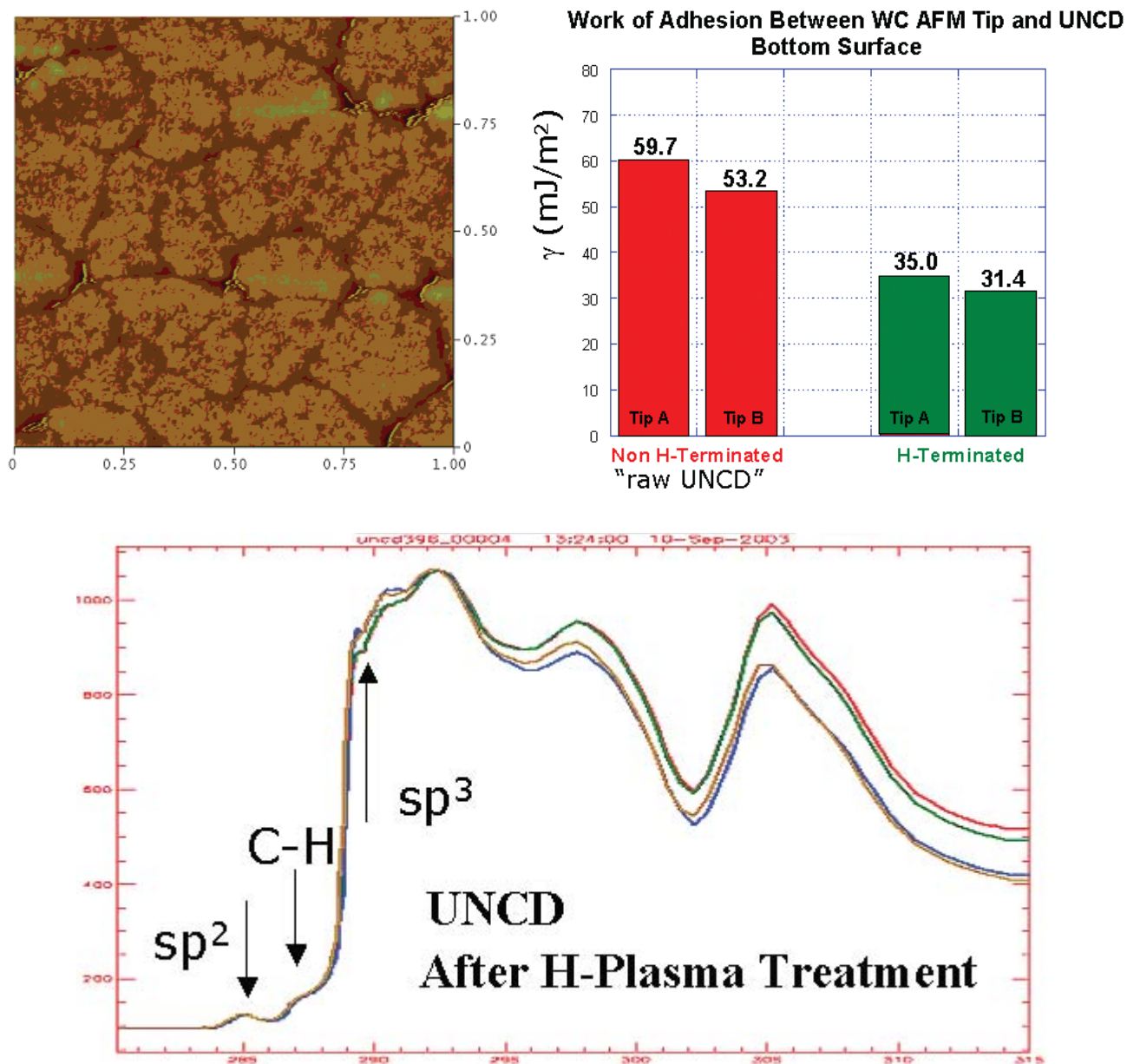


Figure 1. Upper left: $1 \times 1 \mu\text{m}^2$ AFM topographic image of back-side UNCD after H-plasma treatment, revealing supergrains separated by crevices. Height scale=60 nm. Upper right: Adhesion energy measurements with two different tungsten carbide AFM tips on UNCD samples before and after H-plasma termination. Adhesion is consistently reduced by nearly a factor of 2 by the process. Lower figure: NEXAFS spectrum of H-terminated UNCD, taken at the Synchrotron Radiation Center (UW-Madison). The spectrum shows a clear sp^3 peak, with a small sp^2 residual peak (much reduced from the as-grown sample) and a clear C-H bonding peak.

The Effect of Load on Friction and Wear in Hard Carbon Thin Films for MEMS

*M. T. Dugger, and T. A. Friedmann, Sandia National Laboratories, NM
O. Auciello and J. Carlisle, Argonne National Laboratory*

Motivation—Silicon based micromachines with rubbing surfaces suffer from problems due to wear. In an effort to reduce the wear problem, monolayer lubricant coatings have been developed to reduce in-use friction. Though beneficial, these coatings also suffer from wear, thus motivating the search for alternative MEMS materials with improved wear performance. Hard carbon materials such as hydrogenated diamond-like carbon (DLC), hydrogen-free tetrahedral amorphous carbon (colloquially known as amorphous diamond aD), and ultrananocrystalline diamond (UNCD) show low friction and wear under certain sliding conditions and are being studied as possible alternative MEMS materials. Although the friction and wear of these materials have been measured under high load conditions, little work has been done under low load conditions that are closer to loads found at contacting MEMS surfaces.

Accomplishment—A series of experiments have been performed using a linear pin on disc tribometer with a Si_3N_4 ball mated to a flat carbon coated surface under varying environments (dry N_2 , dry air, and 50% relative humidity air) and varying load (9.8, 98, and 980 mN). These loads are still relatively high when compared to contact forces in MEMS devices ($\sim 10 \mu\text{N}$) but are lower than those typically used ($\sim 10 \text{N}$) in conventional tribometers. The wear surface morphology was determined by SEM, and micro Raman spectroscopy was used to characterize the nature of the wear scar and the transfer film formed on the Si_3N_4 ball. The results can be summarized as follows. It was generally found

that the friction coefficient was lowest at the highest load (Figure 1) and that friction increased with *decreasing* load in all environments. The friction coefficient was highest for dry air at the lowest load for both hard carbon films tested. The film in the region of the wear scar retained the character of the bulk film and the transfer film that collected on the ball generally was more graphitic in nature. In general, the development of the transfer film was delayed at the lowest load.

Significance—The low friction values (~ 0.1) typically found for hard carbon materials are usually attributed to the formation of a transfer layer of softer carbon that forms on the mating surface during the run-in period. Low wear performance is usually attributed to the formation of this layer. At the low loads tested in this study, the transfer film formation was delayed and this could have important consequences for hard carbon based MEMS devices where even lower loads are expected. For example, it may be necessary to limit rubbing surfaces to carbon-carbon interfaces where transfer film formation may not be as important. Also, a run in period may be required to set up the proper transfer layer.

Further work needs to be done to fully understand the significance of these results. In particular, studies of self-mated contact at low load and studies of actual carbon-based MEMS devices that are designed to measure friction and wear under true MEMS operating conditions. These investigations are under way.

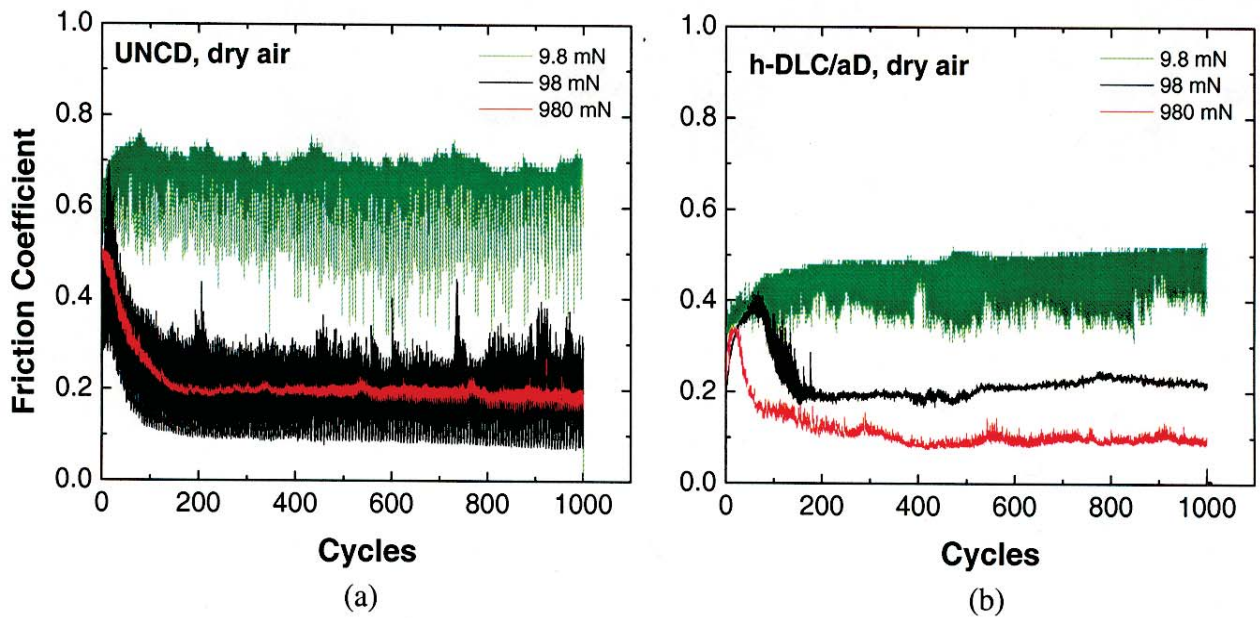


Figure 1. Friction coefficient of UNCD (a) and h-DLC/aD (b) versus rubbing cycle for varying load conditions. Note the increase in friction coefficient with the reduction in load.

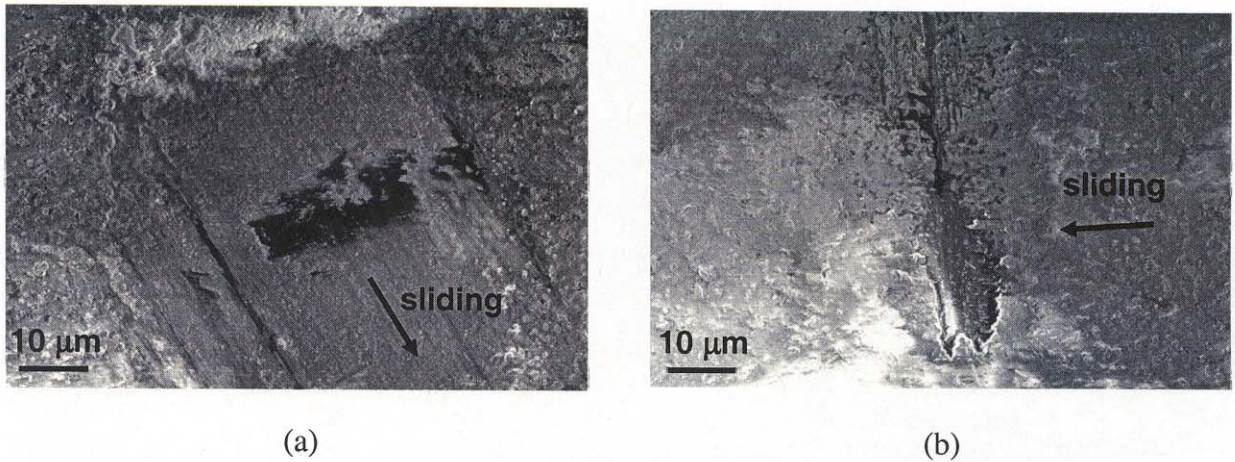


Figure 2. Secondary electron images of wear scars generated during sliding in dry air of a Si_3N_4 ball against UNCD (a) and h-DLC/aD (b) coated flat silicon surfaces. Note the dark patch of transfer film in the contact area of each ball.

Electrostatically Driven Granular Media

Igor Aronson, Argonne National Laboratory
Eli Ben-Naim, Los Alamos National Laboratory
Jeff Olafsen, University of Kansas

Motivation—Characterization of granular media is typically performed using mechanical driving. However, there are several drawbacks with such a driving: often it can not be controlled with high precision and, additionally, the number of particles involved may be small, so statistical fluctuations are significant. This project uses charged microparticles driven by an applied electric field to control the particle dynamics (Figure 1). The project combines experimental and theoretical capabilities with high speed imaging techniques to study dynamical and statistical properties of ensembles of fine powders.

Accomplishment—1) Characterization of coarsening. Electrostatically driven granular media undergo coarsening into growing clusters of circular shape. Using digital imaging techniques, we were able to characterize the cluster size distribution and its dynamics. The process is self-similar, i.e., throughout the system evolution, the size distribution is identical up to a change of scale. We developed a theoretical model in which particles are exchanged between clusters. Predictions of this model regarding the rate by which the coarsening occurs, the overall distribution of sizes and its extremal characteristics are in good quantitative agreement with the experimental data (Figure 2).

2) Characterization of velocity statistics in driven granular media. Using particle tracking methods, we measured the velocity distributions of electrostatically driven granular media. Generally, there are significant deviations from Maxwellian velocity statistics in contrast with ordinary elastic gases. We demonstrated that by focusing on the high energy tails of the velocity distributions (Figure 3), our experimental measurements are in-line with predictions of the kinetic theory with an ordinary thermal heat bath characterizing the energy input at the system boundary. Our theoretical studies show how due to the inelastic nature of the collision, correlations develop between the various components of the velocity and related these correlations quantitatively with the strength of the driving and the degree of inelasticity.

Significance—We have demonstrated that electrostatic driving is a controlled setting for driving granular media and that it allows precise and controlled characterization of granular ensembles. Our coarsening results indicate that the process evolves via exchange of single particle hopping between clusters. Our velocity measurements show that the energy input from the boundary can be faithfully modeled by a thermal heat bath as the correlation between different energy input events is negligible.

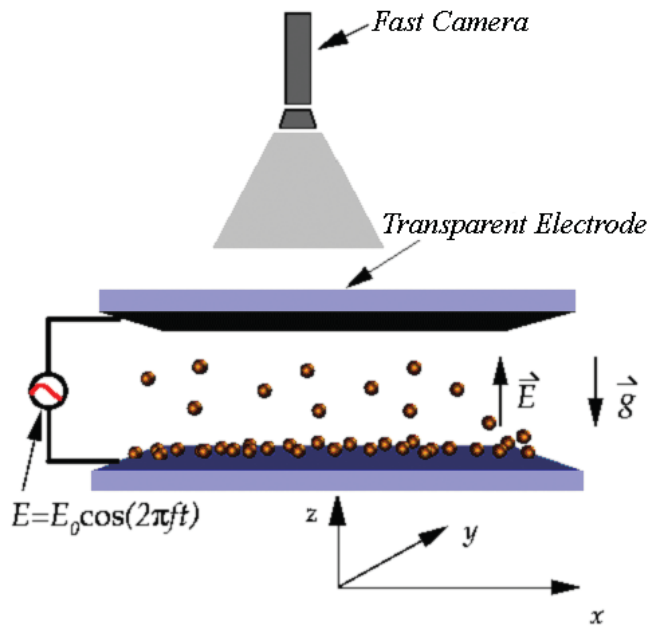


Figure 1. The experimental set-up.

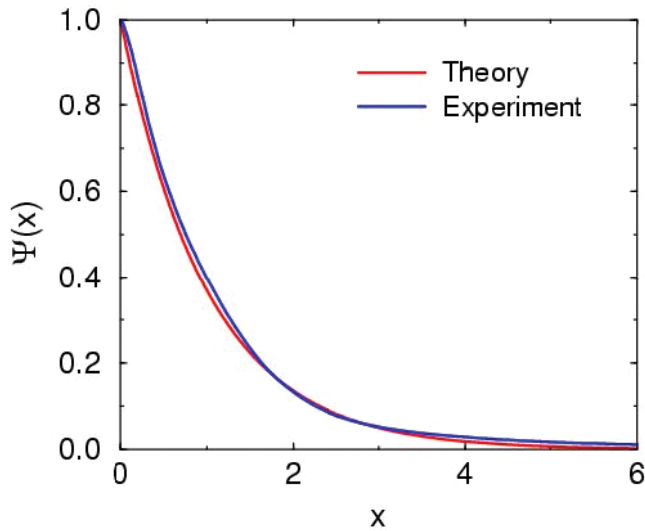


Figure 2. The cumulative area distribution of clusters in the coarsening dynamics. Prediction of the exchange driven growth theory are compared with the experimental data.

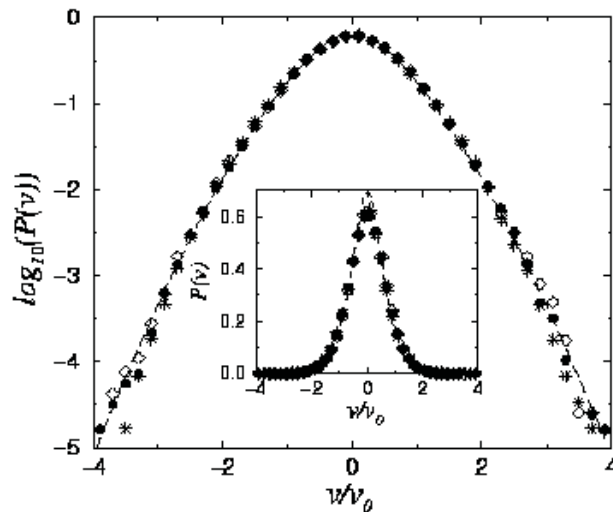


Figure 3. The velocity distributions in electrostatic cell. The velocity distribution is universal, once the variance is set to unity. The high-energy tail is shown in the main figure using a logarithmic scale and the overall distribution is shown in the inset using a linear scale.

Forces in Granular Hopper Flow

*James W. Landry and Gary S. Grest,
Sandia National Laboratories, NM*

Motivation—The flow of granular matter through a hopper has been a long-standing problem of interest in both the physics and engineering communities. Recently, there has been renewed interest in the granular hopper flow problem as an example of the general behavior known as jamming. The concept of jamming was introduced to draw parallels between granular flow, glasses, and foams. All of these systems cease to move (jam) under certain conditions: increasing density for granular materials, decreasing temperature for glasses, and decreasing shear for foams. The flow of granular material from a hopper provides an ideal test bed for testing the predictions of jamming. In addition, there is still no reasonable discrete model for particle flow from a hopper. Our intent is to use our simulations to help develop that model.

Accomplishment—To understand the flow and internal structure of granular hopper flow, we carried out a systematic simulation study of the effect of various parameters using our highly parallel molecular dynamics code. We created hoppers in two geometries, shown in Figure 1, a funnel geometry and a simple cylindrical geometry with a central hole. Results for the dependence of the mass flow rate on radius of the opening for these two geometries are shown in Figure 2 and are in excellent agreement with experiments, so we are confident that we are modeling the physical system appropriately.

The jamming hypothesis predicts that the onset of jamming is signified by a change in the normalized distribution of normal forces $P(f)$ between particles in contact, most notably a deficit in the number of small forces. This results in a peak in $P(f)$ near the average force $f = F / \langle F \rangle = 1$. We determined the distribution of

forces for a range of different openings and found no change in the distribution as the system approaches jamming. We also determined the distribution of impulses $P(i)$, which is measured experimentally, and found that $P(i)$ shows a marked increase at small forces as the system approaches jamming. Impulses measure the total force over the duration of contact, so this measurement contains information on both the duration of contacts and the force of contacts. Both of these results conflict with the present jamming predictions. These results are shown in Figure 3.

The flow properties of the hopper system were also investigated. We find that after subtracting the mean velocity from the flow components, the fluctuations in the particle velocities show non-Gaussian tails, and that there is an asymmetry in the velocity fluctuations in downward direction. There is also a strong coherent motion in the flow, which bears further investigation.

Significance—With our new highly parallel algorithm, we are able to study a wide variety of problems in granular materials. Modeling large systems and obtaining precise information in the bulk of a granular system, which cannot be obtained experimentally is now possible. These simulations suggest ways to refine constitutive relations for analytic models and suggest new types of experiments. In particular, we are now collaborating with Martin Bazant at MIT and Arshad Kudrolli at Clark to test a new model of granular hopper flow - the spot model - with our simulations. Future work will focus on more in-depth investigation of the characteristics of hopper flow and analysis of Couette flow and other geometries.

Contact: Gary S. Grest, Sandia National Laboratories, NM
Phone: (505) 844-3261, Fax: (505) 844-9781, E-mail: gsgrest@sandia.gov

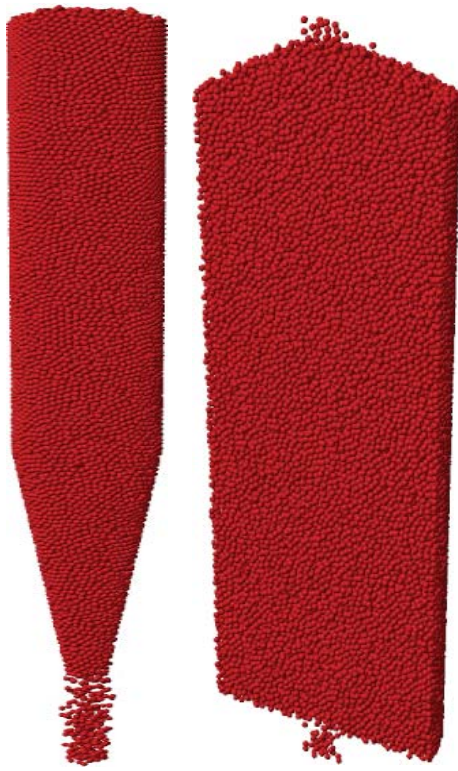


Figure 1. Two different hopper geometries are studied. (a) Mass flow conical hopper with narrowing aperture, with cylinder radius $R=10d$ and aperture radius $r_f = 3d$, where d is the diameter of the particles. Number of particles $N=40,000$. (b) Cylindrical bunker of radius $R=20d$ and aperture of radius $r_f = 4d$ with half of the system removed for illustration, $N=146,000$.

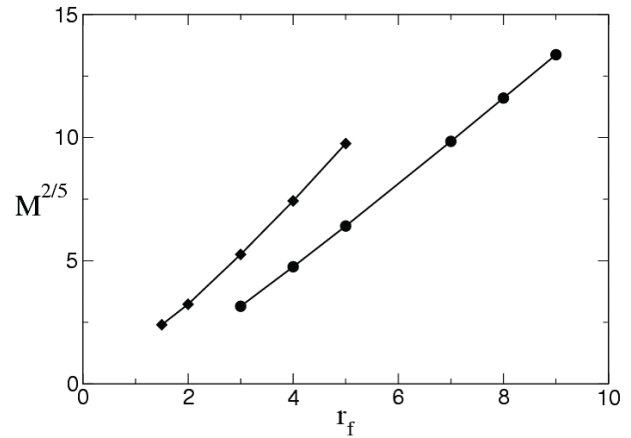


Figure 2. Mass flow rate versus radius of opening, r_f for funnel (squares) and simple cylinder (circles) geometries of Figure 1.

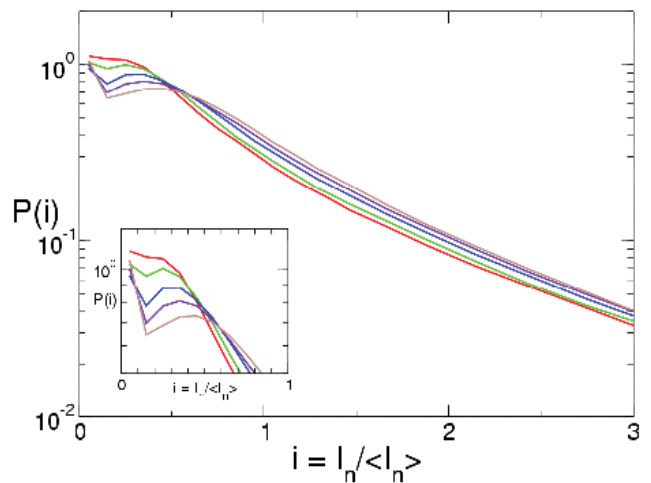
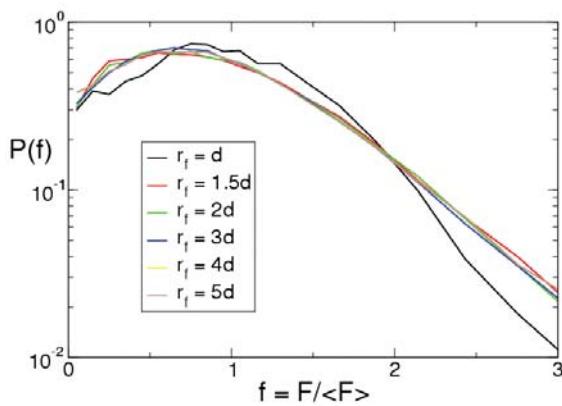


Figure 3. Distribution of (a) forces $P(f)$ and (b) impulses $P(i)$ for the jammed state, $r_f = d$, compared to flowing states $r_f > d$. Note that there is little change in low forces as one approaches jamming (smaller r_f), while there is an increase in low impulses.

Granular Chains: Dynamics of Nonequilibrium Polymers

*Eli Ben-Naim, Zahir Daya, and Robert Ecke,
Los Alamos National Laboratory*

Motivation—The dynamics of granular media involve new challenges. Granular systems can not be modeled using existing equilibrium physics techniques. They are dissipative and must be supplied with energy to counter the dissipation occurring in collisions. Thus, the driving is not thermal. The issue of nonequilibrium driving has been a central concern in modeling granular media. Most notably, it affects our ability to derive constitutive relations, crucial for describing granular flow and packing.

This research, combining experiment and theory, uses driven granular chains as a model for polymers driven out of equilibrium. Having experimental control of the chain driving conditions and ability to measure directly the chain conformation allows characterization of how out of equilibrium polymers explore the available phase space and how topological constraints evolve. Our goal is to answer basic questions such as: does the chain explore all its conformation space uniformly? Is there an effective temperature that characterizes the chain's statistical mechanics?

Accomplishment—1) Diffusion theory of topological constraints. We have shown that even under nonequilibrium driving, effective degrees of freedom governing the relaxation of topological constraints undergo ordinary diffusion. A detailed diffusion theory was developed and its predictions concerning the lifetime of topological constraints such as knots and entanglements confirmed experimentally (Figure 1). 2) Tightening of topological constraints. We

have observed for the first time that topological constraints are localized, i.e., they are most likely to be small compared with the total chain length (Figure 2). An equilibrium theory where all microscopic conformations of the chain are given equal weights is in good qualitative and quantitative agreement with the experimental observations. 3) Spontaneous formation of spirals. We have found that gently vibrated chains may form spirals on their own. This phenomenon occurs in a narrow range of driving conditions and is related to a ratcheting motion induced by asymmetries between the chain ends (Figure 3). This asymmetry induced transport is reminiscent of transport in biological systems. Also, using fast imaging, vibrational motion was studied. It is observed that transverse vibrational modes dominate over longitudinal ones.

Significance—Our experimental system allows direct observation and quantitative characterization of the chain conformation. It allows probing the role of nonequilibrium driving on polymers and on granular media. The results indicate that equilibrium polymer behavior is clearly relevant even under athermal forcing. Thus, polymers driven out of equilibrium may be still modeled by modifying existing equilibrium methods. Computationally, reduced lattice models and molecular dynamics simulations are useful tools for modeling driven granular systems. Granular chains have recently been used by several research groups to model attractive interactions (U Maryland), to measure velocity statistics (U Kansas), and to study chaotic motions (Penn State).

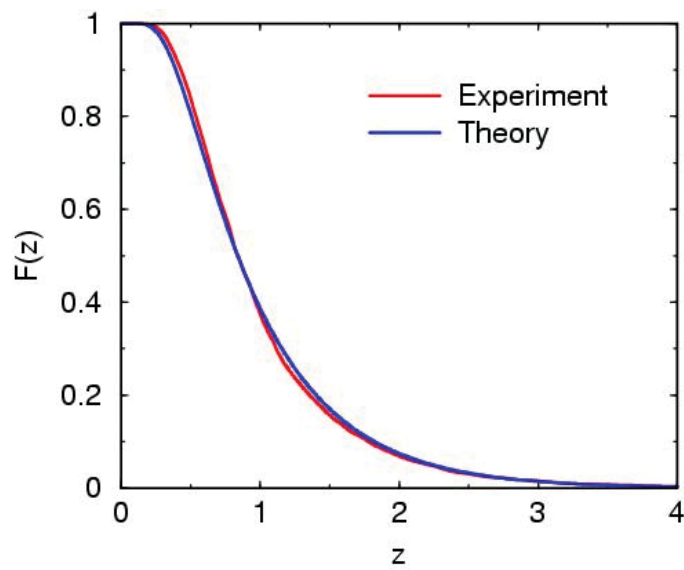


Figure 1. The survival probability of a knot in a vibrated chain. Shown is $F(z)$, the probability the knot remains tied, versus normalized time z . Predictions of the diffusion theory are compared with the experimental measurements.



Figure 2. Conformations of a figure eight. Upon vibration, the size of the loops generally fluctuate. However, configurations where one loop is small and the other large are strongly favored.

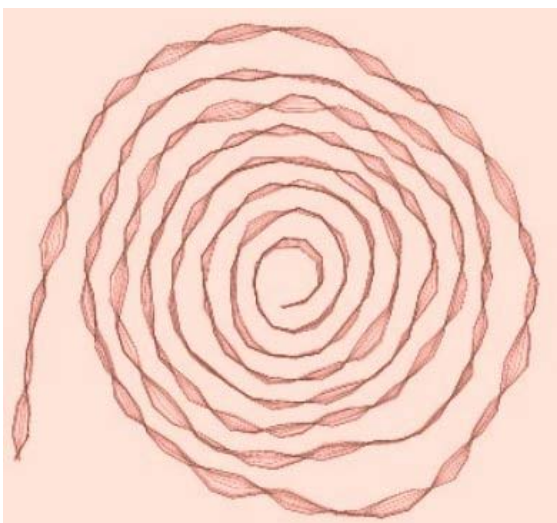


Figure 3. Consecutive conformations of a spiral demonstrating that longitudinal vibrational modes dominate over transverse ones.

Friction between Disordered Self-Assembled Alkylsilane Monolayers

M. Chandross, G. S. Grest, M. J. Stevens, and E. B. Webb III,

Sandia National Laboratories, NM

Motivation—Self-assembled monolayers (SAMs) offer a unique means to alter and control the chemical nature of surfaces. The alkylsilanes are a particularly interesting type of SAM because they bond to oxide surfaces and are thus of use in silicon based micro-electromechanical systems (MEMS), which have a native oxide surface. While experimental measurements yield atomic scale force data, they do not produce the simultaneous structural characterization that can be deduced from molecular scale simulations. A predictive, molecular-level understanding of friction is the missing key to intelligently designing interfacial lubricants for MEMS.

Accomplishment—Molecular dynamics (MD) simulations are ideal for probing the properties of SAM coated surfaces, since they are able to produce both atomic scale force data as well as the underlying structural information. We have carried out extensive MD simulations of the adhesion and lubrication of SAM coated SiO₂ surfaces. We have studied the effects of chain length, system size, shear velocity, and defect density between pairs of SAMs covalently bonded to crystalline and amorphous SiO₂ surfaces. Representative snapshots of equilibrated SAMs with defect densities ranging from zero to 30% are shown in Figure 1. As the surfaces are brought into contact, there is a small region of attraction due to the van der Waals interaction, of about 150MPa for all chain lengths studied, $n = 6$ to 18. Further decrease in the distance between the surfaces leads to compression, as the interactions become strongly repulsive. The relationship between load and surface separation is monotonically dependent on the chain length. Shorter chains are stiffer and have a larger repulsion compared to longer chains. Increasing

defect density at a given chain length also results in stiffer chains, as the increase in area per head-group allows chains to collapse (see Figure 1).

Lubrication between pairs of SAMs is studied by shearing two surfaces relative to each other. The velocities that can be studied by MD are within the range of MEMS devices (on the order of a few cm/s) but large compared to typical force probes. We find that for well-ordered, fully packed SAMs the friction exhibits a non-monotonic chain-length dependence, as seen in the experiments of Salmeron and coworkers. For this case all chain lengths and shear velocities studied show stick-slip dynamics, as seen in Figure 2a. Stick-slip dynamics requires commensurability of the two sliding surfaces, which can be broken by a small percentage of defects, as shown in Figure 2b. Increasing defects leads to increasing friction coefficients in the compressive regime, as determined from the slope of the shear stress vs. normal force. Most friction simulations in the literature determine by dividing shear stress by load at a single state point, which does not account for the attractive region in the force-separation curve, and gives erroneous results.

Significance—MD simulations provide new insight into the atomic-scale motion of SAMs, providing a picture of the molecular structure under shear and a detailed molecular-level understanding of energy dissipation mechanisms. Other work on this project has included varying the end groups to study the chemical dependence of friction and including fluorocarbons. Future work will introduce water into the simulations, leading to a quantitative understanding of adhesion and friction under adverse environmental conditions.

Contact: Michael Chandross, Sandia National Laboratories, NM
Phone: (505) 844-5081, Fax: (505)-844-9781, E-mail: mechand@sandia.gov

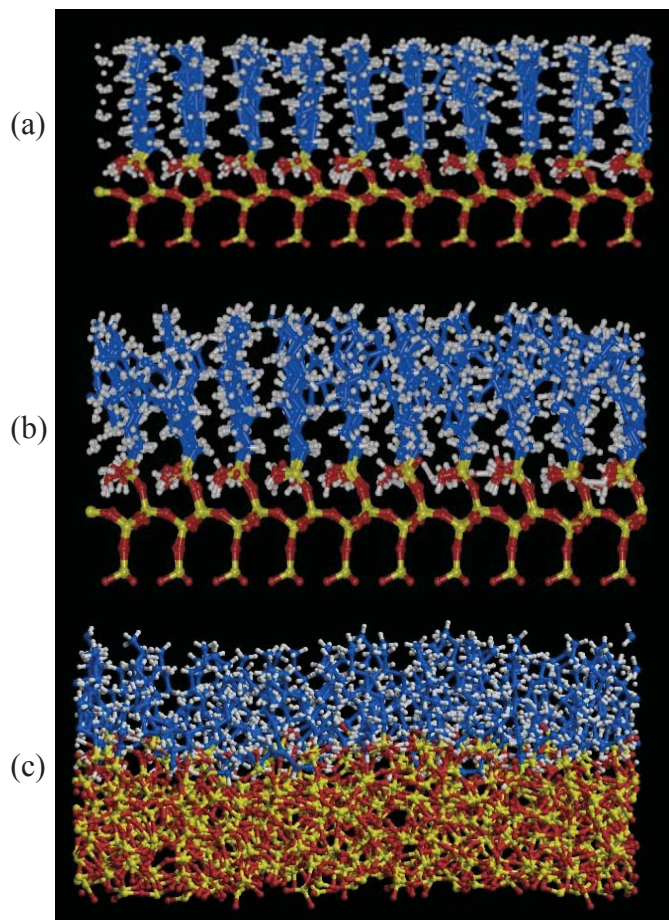


Figure 1. Snapshot of an $n=8$ alkylsilane SAMs with (a) zero (b) 10% and (c) 30% defects. Both (a) and (b) show SAMs on a crystalline substrate while (c) shows a SAM on an amorphous substrate. Silicon atoms are red, oxygen atoms are yellow, carbon atoms are cyan and hydrogen atoms are white.

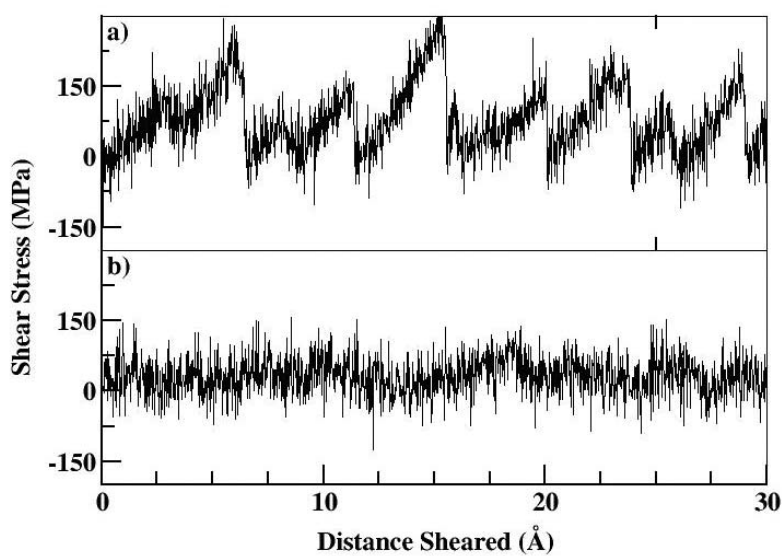


Figure 2. Shear stress as a function of distance sheared for $n=9$ at a normal load of 200 MPa and relative shear velocity $v=0.2$ m/s with (a) no defects and (b) 10% defects. Results for 100 chains attached to each crystalline surface.

Experimentally-Determined Structure and Dynamics in Confined Fluids

Steve Granick, Frederick Seitz Materials Research Laboratory, University of Illinois

James Cowin, Pacific Northwest National Laboratory

Motivation—Molecularly-thin films of fluids constitute the essence of boundary-layer lubrication with relevance to energy applications, among them friction in MEMS devices and the flow of groundwater through porous media. In these cases the large ratio of surface to volume renders friction an unusually large issue, and nanometer thickness raises fundamental issues of the degree to which the known bulk responses extrapolate adequately down to these small dimensions. Better understanding of these issues could lead to improvements in the rational remediation of friction and wear problems, as well as to fundamental advances in liquid state physics.

Accomplishment—At the FS/MRL a unique apparatus was designed and constructed to carry out *in situ* measurements of translational diffusion of films of nanometer thickness, enabling the contrast of viscosity and diffusion within molecularly-thin fluid films [1]. The films are confined between atomically-smooth single crystals. (Fig.1) The main result was that mobility depended remarkably strongly on the local pressure squeezing on the film such that the large deduced activation volume indicated a collective process. The conclusion emerged that friction, an average number, masked a rich pattern of heterogeneous molecular mobility.

Complementary studies at PNNL addressed organic films (3-methyl pentane) constructed using molecular beam epitaxy on a Pt(111) substrate at low temperatures (<30K) [2]. Ions were gently inserted at specific distances from the substrate and the voltage across the film, which is directly proportional to the position of the ions within the film, was monitored electrostatically as the film was heated. Ion motion down the

film was observed at temperatures well below the bulk glass transition temperature. The findings showed that the vacuum/film and film/substrate interfaces did not uniformly change the mobility; they changed it continuously across the film [2].

Significance—These experimental methods have revealed massively heterogeneous dynamics - more rich and complex than appears to have been anticipated by the current notions of "confinement-induced solidification", the term commonly used in this field of study. Heterogeneous dynamics would not be expected if the static friction that these systems display reflected a uniform response across the contact area, as is commonly supposed. Indeed, progress in understanding friction and lubrication has been impeded by the paucity of methods suited for their direct investigation at the molecular level. At the truly molecular level of size definition, the surface forces apparatus and atomic force microscopy play vital roles because they enable direct measurement of static and dynamic forces in liquid films of precisely controllable thickness. Yet though the thickness dimension is molecularly-thin, the area dimension is not, so those force-based measurements represent the ensemble-average of many molecules acting together. Looking to the future, the feasibility of time-correlated fluorescence measurements in a single confined contact, demonstrated here for the first time, will open up a class of experiments not previously possible regarding molecular understanding of lubrication, adhesion, and liquid interfaces in other confined environments.

1. A. Mukhopadhyay, J. Zhao, S.-C. Bae, and S. Granick, *Phys. Rev. Lett.* 89, 136103 (2002).

2. R. C. Bell, H. F. Wang, M. J. Iedema, and J. P. Cowin, *J. Am. Chem. Soc.* 125, 5176 (2003).

Contact: Steve Granick, Frederick Seitz Materials Research Laboratory, University of Illinois
Phone: (217) 333-5720; Fax: (217) 244-2278; E-mail: sgranick@uiuc.edu

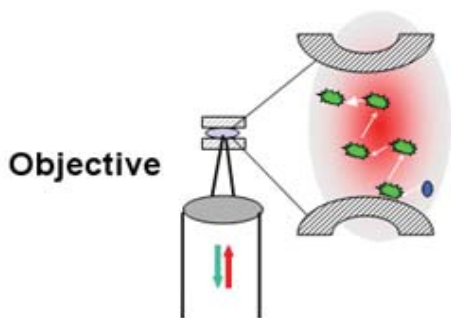


Figure 1. The principle of a newly-invented instrument is to combine friction measurements with fluorescence correlation spectroscopy. Single mica crystals, free of steps, are oriented as crossed cylinders and confined to nanometer spacings with lubricant in between, while at the same time the lubricant contains nanomolar concentrations of fluorescent dyes that are designed to not adsorb. Near-infrared light from a femtosecond laser is focused through a microscope objective and fluorescence is excited by 2-photon excitation. The fluorescence fluctuates as dye molecules diffuse in and out of the femtoliter-sized focal volume. From the rate of fluctuation, the translational diffusion coefficient is deduced [1].

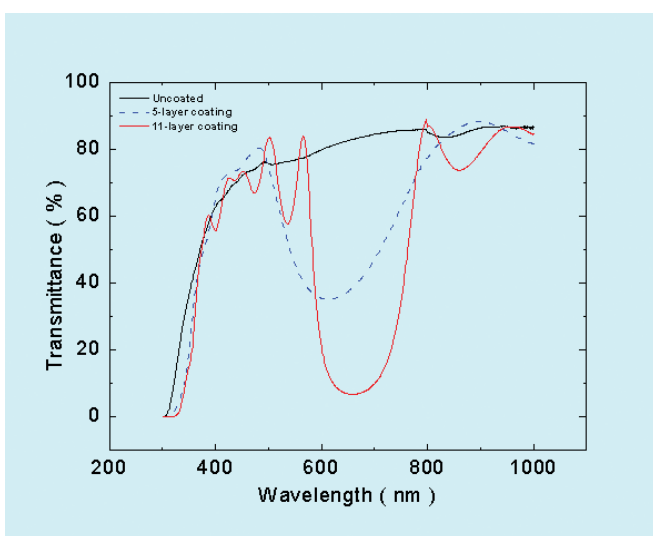


Figure 2. Multiple-layer dielectric coatings on the back sides of the single crystals enable in situ determination of the lubricant thickness by multiple-beam interferometry. Using microfabrication facilities in the FS/MRL, 13 alternate layers of Al_2O_3 and TiO_x produce designed optical properties of high transmittance at 800 nm (for input of femtosecond laser light), high transmittance in the region 400-550 nm (for detection of resulting fluorescence after 2-photon excitation), and high reflectivity in the region 600-700 nm (for multiple beam interferometry).

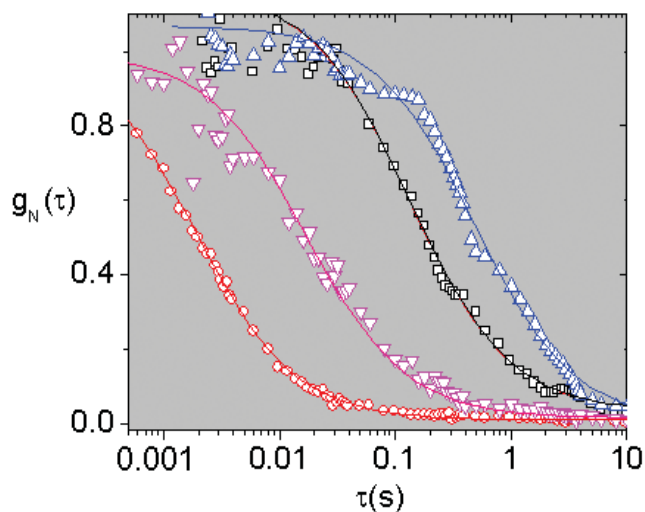


Figure 3. Fluorescence autocorrelation functions, normalized to unity, are plotted against logarithmic time for the fluorescent dye, rhodamine 123, at nanomolar concentrations in 1,2-propane diol films 2.5 nm thick. The focus was at various distances a from the center of the contact and the ratio $x \equiv a/r$ was considered, where r is the contact radius. The symbols denote $x = 0.95$ (red circles), 0.82 (violet down triangles), 0.7 (black squares) and 0.6 (up triangles). Lines through the autocorrelation curves are the least-squares fit to a single Fickian diffusion process. The time to diffuse through the area of laser focus varies by orders of magnitude, indicating that diffusivity slowed by orders of magnitude moving from the edge of the contact zone towards its center.

Control of Friction at the Nanoscale

Y. Braiman, J. Barhen, S. Jeon, V. Protopopescu, and T. Thundat,

Oak Ridge National Laboratory

M. P. de Boer, Sandia National Laboratories, NM

Motivation—Loss of energy and efficiency due to friction is ubiquitous and costs billions of dollars annually. Controlling friction has traditionally been done with lubricants. However, lubricant behavior changes drastically and for the worse when the size of the lubricant film is \sim a few nanometers. With the rapid development of nanotechnology, a different approach to controlling friction is urgently needed.

Accomplishment—We have proposed a new technique [1] whereby friction can be controlled and manipulated during sliding. This technique is based on the concepts of global targeting and non-Lipschitzian terminal attractors. Terminal dynamics has several general consequential properties, namely: (i) very large dissipative forces in the vicinity of the equilibrium points which counteract effectively inertial forces; (ii) finite convergence times to equilibrium points; and (iii) smooth transitions between various regimes, in particular static and kinetic friction.

Figure 1 shows the performance of the proposed technique on a model simulation [1]. Red color lines indicate the time series of the control, while the blue lines show the time series of the velocity of the center of mass. In our simulations, the velocity of the center of mass is inversely proportional to the friction coefficient. We applied the control at time $t = 2000$ and reached and sustained the (arbitrarily chosen) target values. The example in Fig. 1 as well as other examples, clearly indicate that: (i) transient times are very short; (ii) convergence is very fast, and (iii) the strength of the control is small. We performed extensive testing of the proposed algorithm by choosing numerous values of the target velocity. Figure 2 illustrates the performance of the algorithm for different val-

ues of the target velocities as a function of the control amplitude. An experimental setup (Fig. 3) has been implemented to test the proposed technique.

ORNL and SNL researchers are currently testing friction control in the inchworm, a surface micromachined (MEMS) friction device (Fig 4). We derived the equations of motion for the inchworm, and our preliminary results indicate the feasibility of controlling friction of the inchworm during sliding. Our efforts now will explore methods to reduce friction, and demonstrate interesting system dynamics.

Significance—The most significant differences between traditional approaches and those proposed here pertain to robustness, flexibility, and accessibility. In traditional methods, the frictional properties of the lubricant depend on the parameters of the sliding objects (such as the load) and the external forcing and cannot be easily modified during sliding. In our approach, frictional properties of the sliding objects can be modified and controlled during sliding by applying external mechanical or electro-optical perturbations. Moreover, this approach can be implemented in presence or absence of the lubricant.

The efficiency and robustness of the proposed technique are not limited to nanodevices and microelectro-mechanical systems. Our method can be implemented on systems of any size. Thus, this technique has the potential for extremely broad applicability.

1. Y. Braiman, J. Barhen, and V. Protopopescu, *Physical Review Letters* **90**, 094301 (2003).

Contact: Y. Braiman, Oak Ridge National Laboratory

Phone: (865) 241-2065, Fax: (865) 241-0381, E-mail: braimany@ornl.gov

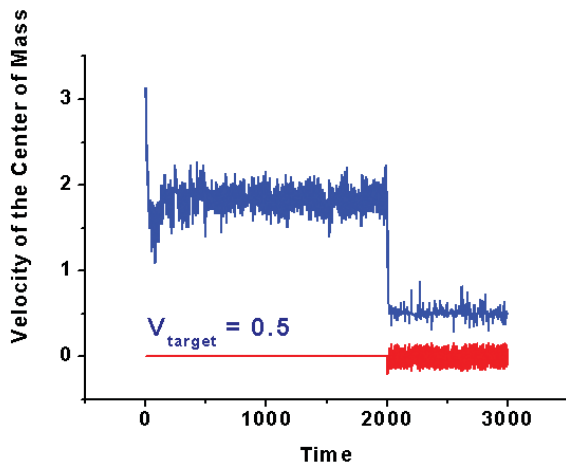


Figure 1. Performance of the control algorithm (computer simulations). We picked a value of the average velocity $v = 0.5$, for $N=15$ particle array. In our simulations, the center of mass velocity is inversely proportional to the friction coefficient. Control was initiated at $t=2000$. Blue lines show time series of the center of mass velocities while red lines show the control. In all cases, the desired behavior was achieved.

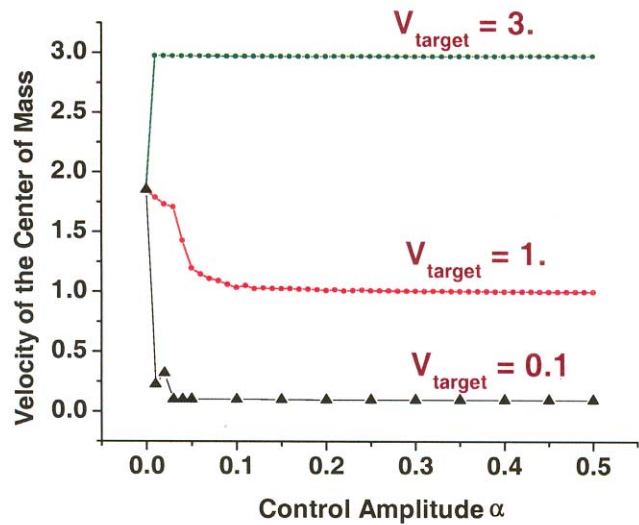


Figure 2. The center of mass velocity as a function of the maximum control amplitude α (computer simulations). Conversion is rapid.

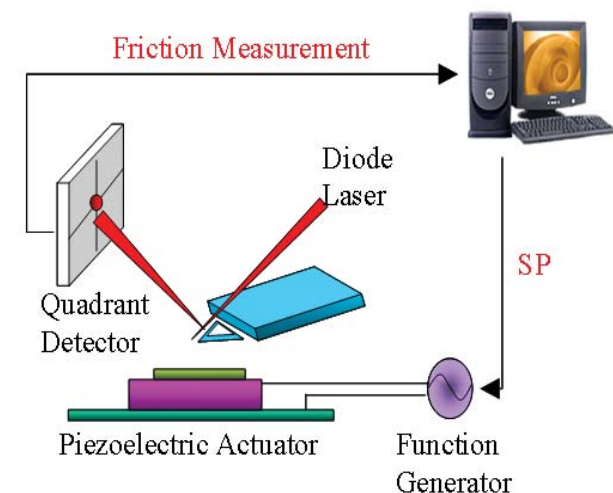


Figure 3. A schematic design of our experimental setup to control friction during sliding. An atomic force microscope with quadrant position sensitive detector is used. A diode laser is focused on the end of the tip and aligned to reflect the laser beam to the center of the detector. As the cantilever scans on the surface, the friction between the lever and surface twists the cantilever and the reflected laser beam moves out from the center position.

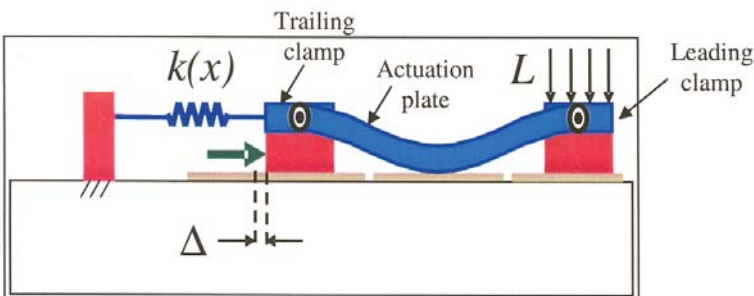
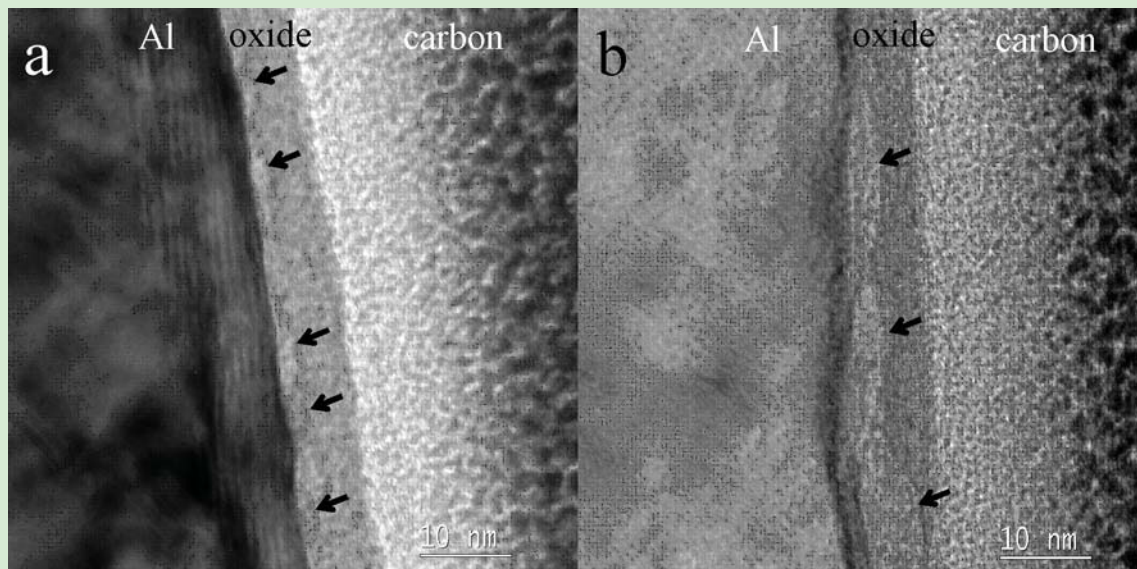


Figure 4. Schematic representation of inchworm, a surface micromachined (MEMS) friction device. The actuation plate is $500 \mu\text{m}$ long, and the friction clamps are $200 \mu\text{m}$ long. To walk it, we apply timed signals to the leading clamp, actuation plate and trailing clamp using large values of L , and each step gives a displacement $\Delta \sim 40 \text{ nm}$. This is a mechanical amplification scheme that achieves high tangential force, allowing friction to be measured over a wide ($\sim 30x$) range of normal load.



The figures on the front and back covers relate to two of the accomplishments described in this issue of *Research Briefs*. In the figure on the front *in situ* X-ray scattering spectra from PbTiO_3 films grown on single crystalline SrTiO_3 substrates reveal superlattice modulations from 180° polarization stripes only down to a 3-unit cell thick film, indicating that 3 unit cells are the lower limit of PbTiO_3 film thickness for the existence of ferroelectricity. This image is from a 4-unit cell thick film (see p. 32).

The above TEM images provide the first experimental observation of nanometer-sized void formation within the passive Al_2O_3 oxide film on Al under pre-pitting electrochemical conditions. The size of these voids (arrows) can be varied by changing the polarization conditions (see p. 38).

SAND2004-0064P: Prepared by the DOE Center of Excellence for the Synthesis and Processing of Advanced Materials at Sandia National Laboratories, Albuquerque, New Mexico 87185 for the Division of Materials Sciences and Engineering, Office of Basic Energy Sciences, U.S. Department of Energy. Sandia is a multiprogram laboratory operated by Sandia Corporation, a Lockheed Martin Company, for the Department of Energy under Contract No. DE-AC04-94AL85000.